A Zonally Averaged Ocean Model for the Thermohaline Circulation.

Part I: Model Development and Flow Dynamics.

Part II: Interocean Circulation in the Pacific-Atlantic Basin System

Daniel G. Wright* & Thomas F. Stocker

C^2GCR Report No. 90-13
September 1990

submitted to

Journal of Physical Oceanography

September 1990

* visiting from: Department of Fisheries and Oceans,
Bedford Institute of Oceanography
Dartmouth, N.S., Canada, B2Y 4A2

A Zonally Averaged Ocean Model for the Thermohaline Circulation.

Part I: Model Development and Flow Dynamics.

Daniel G. Wright* & Thomas F. Stocker

C^2GCR Report No. 90-13
September 1990

submitted to

Journal of Physical Oceanography

September 1990

* visiting from: Department of Fisheries and Oceans,
Bedford Institute of Oceanography
Dartmouth, N.S., Canada, B2Y 4A2

Abstract

A 2-dimensional latitude-depth ocean model is developed on the basis of the zonally averaged balance equations of mass, momentum, energy and salt. Its purpose is to investigate the dynamics and variabililty of buoyancy forced the thermohaline circulation. For the time scales of interest an annual average model is selected, and the momentum balance is taken to be diagnostic. The east-west pressure gradient, which arises upon zonally averaging the momentum equations, is parameterized in terms of the meridional pressure gradient.

The thermohaline circulation is driven by mixed surface boundary conditions, i.e. temperatures are relaxed to prescribed values, while the salt-flux is held constant. The dynamics of the flow is investigated in the geometries of a hemispheric and a global ocean basin both for short and long time integrations extending over many thousands of years. Results are similar to earlier studies by Marotzke *et al.* (1988), Marotzke (1989) and Weaver & Sarachik (1990b,c). In particular, it is possible to perturb a steady state such that a diffusively dominated regime results.

By considering a simple analytic model for the diffusive state in an ocean with a linear equation of state it is demonstrated that any steady, diffusive state is unstable. Convective overturning must occur either at low or at high latitudes. In the former case adjustments are minor, whereas high latitude convection can result in a basin-wide rearrangement of the water masses. These two different processes are verified in the present model; successions of violent overturning occur about every 20,000 years.

The application of the model as a component of a 2-dimensional paleoclimate model is discussed.

1. Introduction

Until recently, the world ocean was commonly considered to play only a passive role as a component of the climate system, simply acting as a reservoir of heat and water. During the last few years, however, new attention has been focussed on the variability of the ocean circulation in relation to climatic change. In particular, the thermohaline circulation has been recognized as a key part in the interactions of the atmosphere, cryosphere and hydrosphere. The implementation of more sophisticated oceanic components into climate models is therefore necessary. In presenting a zonally averaged ocean model, we hope that the present paper is a contribution toward this task.

Studies of the atmospheric circulation and energy balance imply that about 50%, i.e. 2 to 3 PW (1 PW=10^{15} W), of the global meridional heat transport is carried through the world ocean. Unlike in the atmosphere, the heat flux in the ocean is mainly due to the mean meridional overturning, or thermohaline circulation as confirmed by various general circulation models (e.g. Bryan, 1987; Manabe & Stouffer, 1988).

A qualitative understanding of this density driven circulation was provided by Stommel (1961). He demonstrated, using a box model, that two different states of the oceanic system are possible under identical forcing. They correspond to a direct and an indirect circulation, whereby high-latitude cold water is sinking in the former and low-latitude warm but saline water is sinking in the latter. Associated with these states are meridional heat fluxes in different directions. Whereas the direct cell carries heat northward, the opposite is true for the indirect cell.

Rooth (1982) extended Stommel's model including two polar boxes and one

equatorial box with a deep connection between the polar boxes. A three-box model allowing for deep flow between the polar and equatorial boxes was studied by Welander (1986). Of nine possible solutions of the dynamical system four are stable. These are the direct and the indirect symmetric modes and two pole-to-pole circulations with deep water forming either in the northern or in the southern hemisphere.

The Bryan-Cox ocean general circulation model (OGCM) was used by Bryan (1986) to test the validity of the conclusions based on the earlier conceptual box models. He found three different 'steady' states under *mixed boundary conditions*, i.e. surface temperatures are relaxed to specified values, whereas the surface salt flux is fixed. The first state, to which the model converges under *restoring boundary conditions* (both temperature and salinity are relaxed to specified values), shows two hemispheric cells. Deep water is formed at high latitudes in both hemispheres, and upwelling occurs in low latitudes; the meridional heat flux is symmetric. The two other states consist only of one global cell with downwelling in one hemisphere and upwelling in the other. The corresponding meridional heat flux is asymmetric in this case. Manabe & Stouffer (1988) mention that an additional steady state may exist in Bryan's (1986) model. This state has a weak and shallow thermohaline circulation with an intense halocline at high latitudes. Unless salt is added in high latitudes (Bryan, 1986), the symmetric state collapes to this weak circulation.

Marotzke *et al.* (1988) (henceforth MWW) developed a 2-dimensional, zonally averaged ocean model and showed that the symmetric 2-cell circulation is unstable and undergoes a transition to a 1-cell circulation once the boundary conditions are switched from the restoring to the mixed type. Thus both Bryan (1986) and MWW present results which indicate that the symmetric

2-cell circulation obtained under restoring boundary conditions is unstable. Welander (1986), however, predicts this state to be stable; this is due to the lack of vertical structure in the simple box model.

In a later study, Marotzke (1988) demostrated that the collapse of the thermohaline circulation observed by Bryan could be reproduced by the 2-dimensional model of MWW. He then demonstrated the important result that in both 2- and 3-dimensional ocean models, this diffusively dominated state is actually very slowly evolving and eventually exhibits a dramatic instability.

The investigations by Weaver & Sarachik (1990b,c) explore the dynamics of the thermohaline circulation in a 33-level Bryan-Cox OGCM. Long integrations (>7000 surface years, 21,000 bottom years) were performed in both hemispheric and global basins. The model confirms the temporal and spatial variability of the thermohaline circulation; different scenarios are observed such as a succession of violent overturning (*flushes*) occuring on a time scale of a 100 to 1000 years, also decadal variability is present. Eventually, a 1-cell steady state is realized in both basins.

The purpose of this paper is threefold. First, a zonally averaged, latitude-depth ocean model is developed on the basis of the balance equations of momentum, mass, energy and salt. The focus of the model is the thermohaline circulation and its variability. Therefore, seasonal variation is not considered, and the momentum balance allows a diagnostic calculation of the velocity field. The model is related to the one by MWW, however with some physical differences. The most important concerns the parametrization of the east-west pressure gradient that becomes necessary upon zonally averaging the momentum equations. The present model can be coupled to an atmospheric model component to form a 2-dimensional climate model; prelimi-

nary experiments are discussed in Stocker *et al.* (1990).

The second purpose of the paper is to investigate the flow dynamics of the present model under mixed boundary conditions and to verify the findings of MWW, Marotzke (1989) and others. Third, we apply the model in Part II (Stocker & Wright, 1990) to study the interocean thermohaline circulation (Gordon, 1986) in a Pacific-Atlantic basin system.

The paper is organized as follows. Section 2 presents the model development. The numerical procedure is briefly described in section 3. Section 4 deals with the model spin-up and briefly discusses some comparisons with previous thermohaline circulation models using mixed boundary conditions. Section 5 examines the diffusively dominated state and its ultimate instability. Conclusions follow in section 6.

2. Formulation of the two-dimensional ocean model

2.1 Balance equations and boundary conditions

We consider an ocean of uniform depth H and angular width $\Delta\Lambda$. For the space and time scales of interest, the inertial terms are negligible as is friction except where it is required to match specified boundary conditions. It is shown below that horizontal viscosity is not needed to satisfy the conditions of no flow through lateral boundaries, so an appropriate set of momentum and continuity equations in spherical coordinates (λ, ϕ, r) is given by

$$2\,\underline{\Omega} \times \underline{v} = -\frac{1}{\rho_*}\nabla p + \frac{A}{r^2}\frac{\partial}{\partial r}\left[r^2\frac{\partial \underline{v}}{\partial r}\right] \quad , \tag{1}$$

$$\frac{\partial p}{\partial r} = -\rho\, g \, , \tag{2}$$

$$\nabla \cdot \underline{v} + \frac{1}{r^2}\frac{\partial r^2 w}{\partial r} = 0 \quad , \tag{3}$$

where $\underline{v} = (u, v)$ and w are the horizontal and vertical velocity components, $\underline{\Omega}$ is the angular velocity vector of the rotating Earth, p is pressure, ρ_* is a uniform reference density, ρ denotes the density varying in space and time, g is the acceleration due to gravity, $A = 10^{-4} m^2 s^{-1}$ is a constant eddy viscosity and ∇ is the horizontal gradient operator in spherical coordinates.

Several approximations are embodied in (1) - (3). The inertial terms and horizontal diffusion are neglected. The Boussinesq fluid is assumed to be in hydrostatic equilibrium (2). Mass balance and incompressibility lead to (3), describing a divergence free flow. Once the density field is known, eq. (1) - (3) allow the diagnostic determination of the velocity field.

The density is related to temperature and salinity by an equation of state of the form

$$\rho = \rho (T, S) \quad , \tag{4}$$

as given in Gill (1982, p.599, A3.2). Eq. (4) is a potential density referenced to the surface; the pressure dependence is neglected in this study. The balances for heat and salt are

$$\frac{\partial T}{\partial t} + \nabla_\bullet(\underline{v}T) + \frac{1}{r^2}\frac{\partial}{\partial r}(r^2 wT) = \nabla_\bullet (K_H \nabla T) + \frac{1}{r^2}\frac{\partial}{\partial r}\left(r^2 K_v \frac{\partial T}{\partial r} \right) , \tag{5}$$

$$\frac{\partial S}{\partial t} + \nabla_\bullet(\underline{v}S) + \frac{1}{r^2}\frac{\partial}{\partial r}(r^2 wS) = \nabla_\bullet (K_H \nabla S) + \frac{1}{r^2}\frac{\partial}{\partial r}\left(r^2 K_v \frac{\partial S}{\partial r} \right) , \tag{6}$$

where we have used (3) to write (5) and (6) in flux form. K_H and K_v are the horizontal and vertical diffusion coefficients identical for both heat and salt. We select $K_H = 10^3 m^2 s^{-1}$ and $K_v = 0.4, \ldots, 0.8 \cdot 10^{-4} m^2 s^{-1}$.

New dimension-free coordinates are introduced:

$$s = \sin \phi \ , \tag{7a}$$

$$z = (r - a)/H \ , \tag{7b}$$

where a and H are the Earth's radius and the uniform ocean depth, respectively. Noting that $H \ll a$, one can use the approximations

$$\frac{1}{r} \approx \frac{1}{a} \ , \tag{8a}$$

$$\frac{1}{r^2} \frac{\partial}{\partial r} r^2 \approx \frac{1}{H} \frac{\partial}{\partial z} \ , \tag{8b}$$

in (1) - (6). Operating on (1) - (3) and (5) - (6) with the zonal average across the basin extending from longitude λ_W to λ_E,

$$(\overline{\ }) = \frac{1}{\lambda_E - \lambda_W} \int_{\lambda_W}^{\lambda_E} d\lambda \ , \tag{9}$$

and assuming no material or diffusive flux through the eastern and western basin walls, the following set of zonally averaged equations is obtained:

$$- 2 s \Omega \bar{v} = - \frac{1}{\rho_* a c} \frac{\Delta p}{\Delta \Lambda} + \left[\frac{A}{H^2} \bar{u}_z \right]_z \ , \tag{10}$$

$$2 s \Omega \bar{u} = - \frac{c}{\rho_* a} \frac{\partial \bar{p}}{\partial s} + \left[\frac{A}{H^2} \bar{v}_z \right]_z \ , \tag{11}$$

$$\frac{\partial \bar{p}}{\partial z} = - \bar{\rho} g H \ , \tag{12}$$

$$\frac{\partial}{\partial s} \left[c \bar{v} \right] + \frac{\partial}{\partial z} \left[\frac{a}{H} \bar{w} \right] = 0 \ , \tag{13}$$

$$\frac{\partial \bar{T}}{\partial t} + \frac{\partial}{\partial s} \left[\frac{c \bar{v}}{a} \bar{T} \right] + \frac{\partial}{\partial z} \left[\frac{\bar{w}}{H} \bar{T} \right] = \frac{\partial}{\partial s} \left[\frac{c^2 K_H}{a^2} \frac{\partial \bar{T}}{\partial s} \right] + \frac{\partial}{\partial z} \left[\frac{K_v}{H^2} \frac{\partial \bar{T}}{\partial z} \right] \ , \tag{14}$$

$$\frac{\partial \bar{S}}{\partial t} + \frac{\partial}{\partial s}\left[\frac{c\bar{v}}{a}\,\bar{S}\right] + \frac{\partial}{\partial z}\left[\frac{\bar{w}}{H}\,\bar{S}\right] = \frac{\partial}{\partial s}\left[\frac{c^2 K_H}{a^2}\,\frac{\partial \bar{S}}{\partial s}\right] + \frac{\partial}{\partial z}\left[\frac{K_v}{H^2}\,\frac{\partial \bar{S}}{\partial z}\right] \quad , \tag{15}$$

where $c = \cos\phi = (1 - s^2)^{1/2}$, and

$$\frac{\Delta p}{\Delta \Lambda} = \frac{p(\lambda_E, s, z) - p(\lambda_W, s, z)}{\lambda_E - \lambda_W} \tag{16}$$

This quantity cannot be determined from (10) - (16), and an additional parameterization is required to close the system. This will be discussed in section 2.3.

We assume that $\overline{\alpha\beta}$ can be reasonably approximated by $\bar{\alpha}\cdot\bar{\beta}$ for any quantities α and β in (14) and (15). Physically this amounts to neglecting horizontal heat and salt transport due to gyre circulation. As an example consider the North Atlantic and let T′ and V′ be deviations from the zonal mean of the upper-ocean temperature and the upper-ocean northward transport. As $T' > 0$ and $V' > 0$ at the western boundary and $T' < 0$ and $V' < 0$ at the eastern boundary, we have $\overline{T'V'} > 0$ whereas $\bar{T}' = \bar{V}' = 0$. Experiments with general circulation models of the ocean (Meehl *et al.*, 1982, Bryan, 1987) and a coupled atmosphere-ocean GCM (Manabe & Stouffer, 1988) suggest that the northward transport of heat in the Atlantic under present conditions is dominated by the meridional overturning or thermohaline circulation. Based on these results we neglect the meridional transport due to gyres. This may not be a valid assumption when the flow exhibits a very weak and shallow thermohaline circulation.

Boundary conditions have to be specified at the top ($z = 0$) and the bottom ($z = -1$) of the ocean as well as at the northern and southern walls of the basin. At the ocean surface the fluxes of momentum, heat and salt are continuous, and the vertical velocity vanishes in a rigid-lid formu-

lation. For a buoyancy driven ocean we have

$$\left.\begin{aligned} \rho_* A\, u_z &= 0 \quad , && (17a)\\ \rho_* A\, v_z &= 0 \quad , && (17b)\\ w &= 0 \quad , && (17c)\\ -\frac{K_V}{H}\frac{\partial T}{\partial z} &= Q_H \quad , && (17d)\\ -\frac{K_V}{H}\frac{\partial S}{\partial z} &= Q_S \quad , && (17e) \end{aligned}\right\} \quad \text{at } z = 0$$

where the overbars are here and henceforth dropped. The formulation of the boundary conditions here could include the presence of a surface ice cover by appropriately formulating Q_H and Q_S. In such a case, however, (14) and (15) would involve production terms of heat and salt due to melting and freezing of the ice cover. This will be considered elsewhere.

Q_H is the flux of heat from the ocean to the atmosphere (note the sign convention, whereby positive fluxes are strictly upward). For ocean-only runs Q_H represents a heat flux due to Newtonian cooling, viz.

$$Q_H = \frac{H\,\Delta z}{\tau_H}\,(T - T^*) \tag{18}$$

where Δz is the non-dimensional depth of the top grid box, T^* is a prescribed relaxation temperature and τ_H a relaxation time scale for heat. Likewise, the salt flux is expressed as

$$Q_S = \begin{cases} \dfrac{H\,\Delta z}{\tau_S}\,(S - S^*), & (19a)\\ Q_S^* \quad , & (19b) \end{cases}$$

with the relaxation salinity S^* and its time scale τ_S. Q_S^* is a fixed salt flux which may be diagnosed from a previous calculation. The use of (18) in conjunction with (19b) is a standard procedure for climate models and

represents the case of *mixed boundary conditions* (Welander, 1986). They account for the fact that sea surface temperature influences the heat flux (sensible, longwave and latent), whereas sea surface salinity has no instantaneous effect on the salt flux (precipitation-evaporation).

At the ocean bottom (z = -1) a linear friction law is assumed as well as no material or energy fluxes through the bottom. This leads to

$$\left.\begin{aligned} A\,u_z &= r\,H\,u \quad , \\ A\,v_z &= r\,H\,v \quad , \\ w &= 0 \quad , \\ \frac{\partial T}{\partial z} &= 0 \quad , \\ \frac{\partial S}{\partial z} &= 0 \quad . \end{aligned}\right\} \text{ at } z = -1 \qquad \begin{aligned} &(20a) \\ &(20b) \\ &(20c) \\ &(20d) \\ &(20e) \end{aligned}$$

where r is a bottom friction coefficient linearly relating near-bottom velocities to bottom stress (Csanady, 1976; Wright & Loder, 1985). A value of $r = 10^{-4} ms^{-1}$ is selected. At the southern ($s = s_0$) and northern ($s = s_1$) basin walls no-flux conditions on T and S imply

$$\left.\begin{aligned} \frac{\partial T}{\partial s} &= 0 \quad , \\ \frac{\partial S}{\partial s} &= 0 \quad . \end{aligned}\right\} \text{ at } s = s_0,\ s_1 \qquad (21)$$

Note that for the southern and northern walls no conditions on the velocity fields are imposed. No flux through these boundaries follows from (21) by use of the equation of state. From it we have $\rho_s = 0$ at s_0 and s_1, and hence p_s is depth-independent. With the parameterization chosen for Δp (see section 2.3) this holds also for Δp. Thus from (10), (11), (17a,b) and (20a,b) it is apparent that $u = v = 0$ if the wind stress vanishes. Although we will not consider wind forcing in this paper, it should be noted

that by simply setting $\psi = 0$ at the north and south boundaries, the condition $v = 0$ at s_0 and s_1 is automatically achieved without resolving the boundary layer dynamics even if windstress is included (MWW).

2.2 Streamfunction formulation and boundary layer analysis

In solving equations (10) - (21) it is convenient to make use of (13) and introduce the meridional overturning streamfunction ψ defined by

$$v = -\frac{1}{Hc}\frac{\partial \psi}{\partial z} \quad , \tag{22a}$$

$$w = \frac{1}{a}\frac{\partial \psi}{\partial s} \quad . \tag{22b}$$

Differentiating (11) with respect to z, substituting the resulting expression for u_z into (10), and then using (22) to eliminate $\bar{v}$ we obtain

$$\psi_{zzzzz} + (s/\tilde{A})^2 \psi_z = \frac{-H}{2\rho_* a\Omega\tilde{A}} \left[-g H c^2 \rho_{sz} + (s/\tilde{A}) \frac{\Delta p}{\Delta \Lambda} \right] \quad , \tag{23}$$

where $\tilde{A} = A/(2\ \Omega\ H^2)$, and (12) has been used to eliminate $\bar{p}_z$. Eq. (23) is simply another form of the zonal momentum eq. (10).

Boundary conditions for ψ are determined from (17a,b,c), and (20a,b,c). u and u_z are eliminated with the use of (11) to give

$$\left.\begin{aligned} \psi_{zzzz} &= \frac{g H^2 c^2}{2\ \rho_* \tilde{A}\ \Omega\ a}\ \rho_s \quad , && (24a) \\ \psi_{zz} &= 0 \quad , && (24b) \\ \psi &= 0 \quad , && (24c) \end{aligned}\right\} \text{ at } z = 0$$

$$\left.\begin{aligned} \psi_{zzzz} - \frac{r}{2\Omega\tilde{A}H}\,\psi_{zzz} &= \frac{c^2}{2\rho_* \tilde{A}\Omega}\left[\frac{gH^2}{a}\,\rho_s + \frac{r}{2\Omega\tilde{A}a}\,\frac{\partial p}{\partial s}\right], && (25a)\\ \psi_{zz} &= \frac{r}{2\tilde{A}\Omega H}\,\psi_z\ , && (25b)\\ \psi &= 0\ . && (25c) \end{aligned}\right\} \text{ at } z = -1$$

From (23) only five boundary conditions on ψ can be satisfied, and hence one of conditions (24) and (25) must be redundant for consistency. Indeed, integrating (23) over the water column and using (24a,b) and (25c) it follows that (25a) is a redundant condition. In fact, any one of (24a,c) and (25a,c) may be shown to be redundant with respect to the remaining equations.

In principle (23) could now be numerically solved in $-1 \le z \le 0$ by employing a shooting technique, (e.g. Runge-Kutta). However, we note that

$$\tilde{A}^2 = \left(\frac{A}{2\Omega H^2}\right)^2 \approx \left(\frac{10^{-4}}{2\cdot 7\cdot 10^{-5}\cdot 25\cdot 10^{6}}\right)^2 \approx 8\cdot 10^{-16}\ . \qquad (26)$$

Since homogeneous solutions of (23) vary exponentially on a (non-dimensional) scale of order $(\tilde{A}/s)^{1/2}$, small inaccuracies grow rapidly away from the initial point making this approach impractical.

For a boundary layer analysis (23) is integrated once with respect to z to obtain

$$\tilde{A}^2\,\psi_{zzzz} + s^2\,\psi = F(s,z)\ , \qquad (27)$$

with

$$F(s,z) = s^2 B_0 + \frac{H}{2\rho_* a\Omega}\left[\tilde{A}\,g\,H\,c^2\rho_s - s\int_{-1}^{z}\frac{\Delta p}{\Delta\Lambda}\,dz\right]\ , \qquad (28)$$

and B_0 is an arbitrary function of s that will be determined by the boundary conditions. Consider the upper boundary layer, in which we write

$$\psi = \psi^I + \psi^B \quad , \tag{29}$$

where ψ^I is an interior solution constant within the boundary layer, and the boundary layer contribution ψ^B vanishes in the interior. There, equation (27) becomes

$$s^2 \psi^I = F(s,z) \quad , \tag{30}$$

accurate to order $(\tilde{A}/s)^2$, indicating that this analysis holds except approaching the equator. Inserting (29) into (26), using (30) and neglecting variations in ψ^I within the boundary layer, we obtain in this region

$$\tilde{A}^2 \psi^B_{zzzz} + s^2 \psi^B = 0 \quad . \tag{31}$$

Introducing the boundary layer coordinate $\xi = z/\tilde{A}^{1/2}$, yields

$$\psi^B_{\xi\xi\xi\xi} + s^2 \psi^B = 0 \quad , \tag{32}$$

with the solution

$$\psi^B = e^{\tilde{\mu}\xi} \quad ; \quad \tilde{\mu}^4 = - s^2 \quad . \tag{33}$$

Of the 4 solutions in (33) only two remain bounded in the interior where $\xi \to - \infty$; the other two solutions must vanish identically. Similarly, two independent solutions are obtained in the bottom boundary layer. This leads, upon rescaling, to

$$\psi = \frac{1}{s^2} F(s,z) + \sum_{j=1}^{4} B_j e^{\mu_j (z - z_j)} \tag{34a}$$

$$\mu_{1,2} = (1 \pm i) \cdot \left[\frac{s}{2\tilde{A}}\right]^{1/2} \quad , \quad z_{1,2} = 0 \quad . \tag{34b}$$

$$\mu_{3,4} = -(1 \pm i) \cdot \left(\frac{s}{2\tilde{A}}\right)^{1/2} \quad , \quad z_{3,4} = -1 \ . \tag{34c}$$

where the 5 coefficients B_0, B_1, ..., B_4 are to be determined from the boundary conditions (24) and (25) and will be functions of s.

In fact, we need only determine B_0, since the other terms in the homogeneous solution will not be resolved by the finite vertical resolution. This is guaranteed for a vertical resolution coarser than 50 m. With B_0 determined and $\psi = 0$ at $z = 0, -1$ the solution will be effectively completed. Note that (24) involves only B_0, B_1 and B_2 while (25) involves only B_0, B_3 and B_4. Hence either of these may be used to determine B_0. Assuming a constant ψ_I within the boundary layer, (24a) gives

$$B_1 + B_2 = - \frac{\tilde{A}\, g\, H^2 c^2}{2\, \rho_* \Omega\, s^2 a}\ \rho_s \ , \tag{35}$$

and then (24c) provides

$$B_0 = B_1 + B_2 - \frac{1}{s^2}\ F\,(s,0) \ . \tag{36}$$

Although F(s,0) still contains $\Delta p/\Delta\Lambda$, the integral over the basin depth can be calculated from (10) to be

$$\int_{-1}^{0} \frac{\Delta p}{\Delta \Lambda}\ dz = - \frac{\rho_* a\, c}{H}\ r\ u(s,-1) \approx 0. \tag{37}$$

Here we have used (17a) and (20a) and taken $u(s,-1) = 0$, hence neglecting the contribution of the bottom Ekman layer to the total north-south mass transport. Using (37) in (28) to determine F(s,0) and replacing it in (36) we obtain

$$B_0 = 0 \quad . \tag{38}$$

In summary, for a grid that does not resolve the top and bottom boundary layers the streamfunction ψ is given by

$$\psi\ (s,z) = \frac{H}{2\ \rho_* a\ \Omega\ s^2} \left[\tilde{A}\ g\ H\ c^2 \rho_s - s \int_{-1}^{z} \frac{\Delta p}{\Delta \Lambda}\, dz \right] \quad , \tag{39}$$

in the interior and $\psi(s,0) = \psi(s,-1) = 0$. The first term on the r.h.s. of (39) represents the frictionally induced flow associated with vertical gradients in the internal stress Av_z, while the second term is the geostrophic flow due to the east-west component of the pressure gradient. A parametrization of this pressure gradient in terms of known quantities eventually allows us to calculate ψ. This will be presented in the following section.

Finally, we note that (39) does not hold at the equator. In the present study the grid has always been chosen such that ψ need not be determined at $s = 0$. In global runs the central grid cell straddles the equator, while in hemispheric runs we set $\psi = 0$ at the equator as a boundary condition.

2.3 Parameterization of the east-west pressure gradient

The model formulation can only be completed if Δp in (39) is linked with the other variables in the model. This problem has been recognized previously by MWW, but their approach is different from the considerations here. The two parametrizations will be compared below.

One limiting case is an ocean which is unbounded (and hence cyclic) in the east-west direction. For this case $\Delta p = 0$, and it follows from (10) and (11) that the zonally averaged north-south flow reduces to that associated with stresses acting on the nearly geostrophic zonally averaged east-west flow. The meridional circulation is thus very weak and a poor approximation

to that in a zonally bounded basin. This case was examined by Bonsell (1988) but is not relevant to the time scales of interest here, for which advection by the meridional circulation is critically important.

A second tractable limiting case is an ocean basin which is so narrow that the east-west flow is negligible (Källèn & Huang, 1987). Setting $\bar{u} = 0$ in (10) and (11) one finds

$$\frac{A}{H^2} v_{zz} = \frac{A}{2 \rho_* H^2 \, a \, c \, \Omega \, s} \frac{\Delta p_{zz}}{\Delta \Lambda} = \frac{c}{\rho_* a} \frac{\partial p}{\partial s} \quad . \tag{40}$$

Again this allows us to determine $\Delta p/\Delta \Lambda$. In this limit $\partial p/\partial s$ drives the meridional circulation directly rather than being largely balanced by the Coriolis force associated with the east-west flow as is the case for a wider basin. Equation (40) is thus not applicable to wider basins. One possible solution to this problem is to artificially increase the value of A so that v is reduced to an acceptable range. This yields the parameterization considered by MWW which will be discussed further below.

For an ocean of intermediate width, a relation between the two components of the pressure gradient is suggested by considering again the momentum equations (10) and (11) with the eddy diffusion neglected in (10) and replaced by linear damping $-\mu\bar{v}$ in (11) (Killworth, 1985). Solving for $\Delta p/\Delta \Lambda$ we obtain, dropping the overbars,

$$\frac{\Delta p}{\Delta \Lambda} = - \, 2 \, \epsilon \, s \, c^2 \, \frac{\partial p}{\partial s} \quad , \tag{41}$$

where

$$\epsilon = \frac{\Omega}{\mu} \left(1 - \frac{u}{u_g} \right), \tag{42}$$

and the zonally averaged geostrophic velocity u_g is defined by

$$u_g = -\frac{c}{2\,\rho_* a\, s\, \Omega}\frac{\partial p}{\partial s} \quad . \tag{43}$$

For a narrow basin $u/u_g \approx 0$ and ϵ is simply the ratio of the damping to the inertial time scale. For a constant value of $1/\mu = 3$ days (Killworth, 1985) this limit gives $\epsilon \approx 20$. In a realistic ocean basin which is many inertial Rossby radii across, we expect that u will be almost equal to u_g so ϵ would be greatly reduced.

Although we expect ϵ to be generally positive, it may vary spatially. Nevertheless, as a closure we have chosen to investigate the parameterization (41) with ϵ simply fixed at a constant value. Note that this parameterization yields reasonable results at the equator as well as at the poles. Near the equator we have $\Delta p/\Delta\Lambda \sim s\ \partial p/\partial s$ indicating proportionality to f, the Coriolis parameter. The meridional velocity v stays finite at the equator without incorporation of new dynamics. At the poles $\Delta p/\Delta\Lambda \sim c^2\ \partial p/\partial s$ tends to zero. Likewise, $v \sim c\ \partial p/\partial s$ tends to zero at the poles.

It is of interest to compare (41) with the parametrization used by MWW:

$$\frac{A_*}{H^2}\, v_{zz} = \frac{c}{\rho_* a}\frac{\partial p}{\partial s} \quad . \tag{44}$$

As noted earlier, this result is formally equivalent to (40) but with A replaced by A_*. Order-of-magnitude considerations require $A_* \approx 10^2 \ldots 10^3 m^2 s^{-1}$, whereas A is of order $10^{-4} m^2 s^{-1}$. The alternative parameterization (41) and the geostrophic approximation to v yields

$$-\frac{\Omega}{\epsilon}\, v = \frac{c}{\rho_* a}\frac{\partial p}{\partial s} \quad . \tag{45}$$

While (44) and (45) arise from different approaches, the correspondence is evident. Indeed, substituting $v \sim \cos \pi z$ (accounting for the rough structure of the meridional velocity field) into both (44) and (45), and

comparing results leads to

$$\epsilon \approx \Omega H^2 / \pi^2 A_* \quad . \tag{46}$$

For $A_* = 6 \cdot 10^2 m^2 s^{-1}$ (MWW) and $H = 5000$ m we obtain $\epsilon = 0.31$ which is consistent with independent estimates of order 0.2 to 0.5 discussed below.

The consistency suggested by the above comparison is limited. The fundamental differences arise from the fact that the MWW model is essentially non-rotating and must use a large value of the vertical diffusivity A_* for compensation. This eliminates any possibility of return flow being carried in a relatively thin suface layer. The presence of these boundary layers is central to the formulation here, and represents an extension of the earlier model. Further, Earth's rotation, spherical geometry and the β-effect are included in the present model, whereas these effects are reflected solely by the large value of A_* or neglected entirely by MWW.

To test the validity of (41) and estimate an appropriate value for ϵ, two different approaches were used. Initially, we performed a series of model runs with ϵ varying and all other model parameters fixed. The details of some of these runs are discussed in section 4.1. From this series of runs it was determined that, for the model parameters considered, a value of $\epsilon = 0.5$ yielded a reasonable meridional overturning rate of order 10 Sv (1 Sv = $10^6 m^3 s^{-1}$).

Regarding the validity of (41), the above approach allows us only to state rather subjectively that this parameterization yields 'reasonable' looking results. A more stringent test of the form of (41) and an estimate of ϵ based on more realistic forcing was obtained using results from the 3-dimensional Bryan-Cox OGCM study by Weaver & Sarachik (1990a). They determined a steady state circulation in a 60° wide hemispherical basin by re-

storing surface temperature and salinity to zonally averaged Levitus (1982) data and applying a realistic wind stress. This steady state (Weaver & Sarachik, 1990a, Fig. 4b) was integrated for another 2630 surface years with no wind forcing yielding a practically identical thermohaline circulation (A.J. Weaver, pers.comm.). This aside suggests that Ekman pumping due to surface wind stress is not an important forcing for meridional overturning.

Unfortunately pressure is not a standard output from the OGCM, so (41) was differetiated with respect to z (thus replacing p by ρ) and integrated from the surface down to obtain the relation

$$\int_0^z \frac{\Delta\rho}{\Delta\Lambda}\,dz = -2\,\epsilon\,s\,c^2 \int_0^z \frac{\partial\rho}{\partial s}\,dz \quad , \tag{47a}$$

or equivalently

$$\frac{\Delta(p - p_s)}{\Delta\Lambda} = -\epsilon\left[\,2\,s\,c^2\,\frac{\partial}{\partial s}\,(p - p_s)\,\right] \tag{47b}$$

Values of the integrals in (47a) were determined at each latitude and each vertical level of the model. Finally, at each level all but the three northern and southern (6° latitude) values were used to obtain a least squares estimate of ϵ and the correlation coefficient between the left and right sides of (47b). Individual estimates of ϵ from the six neglected cells were generally within a factor of two of the least squares estimates, but they did significantly reduce the correlation coefficient. Fig. 1 shows relation (47b) at 570m (×) and 2135m (+) depth; the estimated ϵ are 0.163 and 0.182, respectively. The estimates of ϵ (×) and correlation coefficients (+) as functions of depth are displayed in Fig. 2. Below 500m a constant value of $\epsilon \approx 0.2$ is appropriate. High values of the correlation coefficients indicate that the latitudinal structure of the relationship between the pressure gradient components is accurately approximated by (41).

The apparent degradation towards z = 0 is somewhat misleading. Recalling that results were obtained from a run with surface values relaxed to zonally averaged data, we note that, since $\Delta\rho \to 0$ at z = 0, ϵ must tend to zero there. Vertical diffusion will convey this effect to deeper levels, so we expect ϵ to decrease smoothly to zero at z = 0 as observed. Since both left and right sides of (47) vanish at z = 0, it is also not surprising to find a low correlation coefficient there: local shears should not be expected to be accurately modelled by (47).

Finally, we note that if the transport carried below 500m is accurately estimated using (47), then the net transport above 500m must also be accurately determined since the sum over the two regions vanishes. Thus, while details may be poorly represented, (47) should give a useful approximation to the overall vertical structure of the meridional circulation throughout the water column.

3. Numerical solution procedure

A solution of equations (10) - (15) is conveniently achieved by use of the meridional overturning streamfunction introduced in section 2.2. The diagnostic equation for the streamfunction (39) and the prognostic advection-diffusion equations (14) and (15) for temperature and salinity are solved on a uniform grid spanning the (s,z)-coordinates with N vertical layers each containing M grid boxes. The flux fields are calculated on the box walls whereas the volume fields are taken centered. For N = 20 the top layer of 250 m is represented only by its average temperature and salinity fields. This is not satisfactory for the calculation of surface fluxes and later coupling to an atmosphere model. Thus, a linear extrapolation of T and S is used to estimate surface values.

The first step of the numerical procedure is to calculate the density gradients. Centred differences are used to estimate values at interior cell boundaries. Normal derivatives vanish at the bottom, north and south boundaries, and values at the surface are consistent with the linear extrapolation of T and S to the surface. Values within cell boundaries are obtained by linear interpolation. The meridional overturning transport is then diagnosed in a vertical column using the imposed boundary conditions. With the velocity field known, the advection-diffusion equations (14) and (15) are solved by applying the numerical scheme of Fiadeiro & Veronis (1977) for calculation of the fluxes across cell boundaries. Simple forward differencing is used in the time domain. With T and S determined, ρ is obtained from (4). A non-diffusive convection scheme is used to ensure complete mixing of unstable water masses after a finite number of iterations.

4. Spin-up and test runs

The standard procedure of ocean spin-up is applied. Basic model parameters are given in Table 1. Integration starts from an ocean at rest with uniform temperature T = 7°C and salinity S = 35 ppt. The circulation is set up by thermal and haline surface forcing. T and S at the ocean surface are relaxed to specified values T^* and S^* on a time scale of 100 days. The following analytic forms are used:

$$T^* = (1 + \cos(\pi\, s)) \cdot 12.5^{\circ}C, \tag{48a}$$

$$S^* = (36 + \cos(\pi\, s)) \cdot \text{ppt} . \tag{48b}$$

With these values, the temperature effect dominates the equator-to-pole density difference by about a factor of three compared to the salinity effect, so the resulting meridional circulation is downwelling at the poles.

Although (48a,b) are chosen to be qualitatively consistent with observations, they are obviously crude. To obtain a meridional overturning rate of order 10 Sv we have taken $\epsilon = 0.5$ throughout the remainder of this paper.

The system is near equilibrium after a few hundred years but the integration is carried out to 5050 yr. The final equilibrium is shown in Fig. 3. The 2-cell circulation is in qualitative agreement with the results of Bryan (1986), MWW and Weaver & Sarachik (1990b). A conspicuous contrast to the circulation of MWW is that the meridional flow feeding the region of deep water formation is surface trapped (Fig. 3). This is a phenomenon that also occurs in the zonal averages of 3-dimensional OGCMs and suggests that the model here reproduces the qualitative features of the meridional deep circulation fairly realistically.

Starting from the spun-up equilibrium state described above, the vertical surface salt flux Q_S^* was diagnosed (Fig. 3d) and used as the surface boundary condition on salt (19b) henceforth. The temperature field was still relaxed to (48a) forming the usual *mixed boundary conditions*. Experiments adding a 0.2 ppt positive (negative) salinity anomaly to the surface north of 38°N (south of 38°S) and a control run were performed. Integration was continued for an additional 2500 y.

The results were generally consistent with previous studies (MWW; Bryan, 1986), and details are not shown here. The most important conclusion is that the symmetric circulation in Fig. 3 is unstable under mixed boundary conditions. In all three experiments a new steady state was established, which consisted of a single cell with deep water formation in high latitudes (Fig. 4, control run).

The instability of the direct symmetric circulation demonstrated here and by MWW contrasts with the stability of the direct symmetric circulation

determined by Welander (1986) using a simple three-box model with no vertical resolution. To illustrate the origin of this difference, consider the consequence of adding some salt to one of the polar cells in Welander's model. The density of the polar cell increases so that the advective exchange of water between the polar and equatorial boxes increases. However, the decreased salinity contrast between the boxes causes the advective exchange of salt to decrease. Consequently the forcing associated with Q_S^* dominates that due to advection and shifts the salinity back toward its original equilibrium, resulting in a stable equilibrium. In models with multiple vertical levels the situation is different. The addition of salt to the surface cell of the polar box still results in an increase in the advective exchange of water, but now the salinity of the deep water in the polar box is unchanged, so that there is no immediate change in the salinity of the water being exchanged between high and low latitudes. The increased circulation thus leads to a further increase in polar salinity. The perturbation is enhanced, leading to instability of the direct circulation.

5. Thermohaline catastrophe and subsequent evolution

5.1 Hemispheric basin

We now study the present model in the restricted geometry of a hemisphere to re-examine the results of Marotzke (1989). The the basin is 5000 m deep and extends from 0° to 80°N with 60° angular width, and a 10 (horizontal) $\times$ 20 (vertical) grid is chosen. The steady state under restoring boundary conditions is shown in Fig. 5a, from which a control run and a perturbation experiment continue both under mixed boundary conditions.

Figure 5b shows the circulation of the control 5000 years later. The adjustment is minor; the maximum transport increased by about 15%. This

increase occurred abruptly about 100 years after the change in boundary conditions, and the transients, whose initial peak-to-peak amplitude were about 1 Sv, had become negligible a few hundred years later. The state shown in Fig. 5b has not changed significantly over the last 4000 yr of integration. This shows that there is a stable equilibrium under the mixed boundary conditions which is very similar but not identical to that under the restoring boundary conditions.

The situation is different when a small negative salinity anomaly of 0.1 ppt is added north of 36°N. The time series of the maximum and minimum stream function over 80,000 years of integration (Fig. 6) show that 600 years after the freshening of the region of deep water formation the positive circulation has collapsed, and now consists of a shallow, indirect cell located at low latitudes (Fig. 7a). The collapse is due to the process described by Bryan (1986). The state found here is in qualitative agreement with the 3-dimensional results presented by Marotzke (1989). Analysis of the surface heat flux reveals a net uptake of heat through the surface implying subsequent adjustments. About 20,000 years later the circulation has deepened but is even weaker now (Fig. 7b). The most striking change, however, can be attributed to the heat input which causes the deep ocean to warm up by some 13°C. The surface-to-bottom density contrast decreases from 2.4 kgm^{-3} (t = 8000 yr) to 0.2 kgm^{-3} 20,000 years later.

The consequence of this long-term process is the dramatic event at t = 28620 yr (Fig. 6), when massive convective mixing at high latitudes sets in and accelerates the circulation to a maximum of 380 Sv (Fig. 7c). The violent circulation is basin-wide and causes major rearrangements in the temperature and salinity fields. The downwelling in high latitudes releases very effectively all the heat taken up during the previous millenia at rates

exceeding 400 Wm^{-2}. Immediately after the period of very rapid changes, there is a period of about 2000 yr when the circulation is variable but generally similar to that illustrated in Fig. 5. This state eventually collapses, returning to a state similar to that shown in Fig. 7. The above process repeats itself two more times during the next 50,000 years of integration (Fig. 7).

These so-called *flushes* (transports exceeding 200 Sv) were first reported by Marotzke (1989) in both 2- and 3-dimensional hemispheric ocean models. The 3-dimensional OGCM of a global basin by Weaver & Sarachik (1990b) shows a sequence of less violent flushes (50+ Sv) recurring on a time scale of 200 to 1000 years, which eventually give way to a remarkably steady state. This time scale hints at an operating process that may be different from vertical diffusion important in Marotzke (1989) and the experiments presented here.

5.2 Instability of the purely diffusive steady state

When the circulation is collapsed to the state in Fig. 7a, advective and convective processes are no longer important; instead the evolution is dominated by diffusion. Both T and S in the deep ocean will tend to the average surface values with negligible latitudinal structure. This leads to a stabilization with respect to temperature and a destabilization with respect to salinity of the equatorial water column. The opposite happens in the polar water column.

To obtain a quantitative understanding of the important processes we consider a simple diffusive model. Let y and z be dimensional coordinates for latitude and depth, and consider the T and S fields corresponding to a diffusive equilibrium governed by

$$K_H T_{yy} + K_V T_{zz} = 0 , \tag{49a}$$

$$K_H S_{yy} + K_V S_{zz} = 0 , \tag{49b}$$

in a basin of depth H and length L. Applying mixed boundary conditions at the surface z = 0 of the form

$$T = T_0 \cdot \left(1 + \cos \frac{\pi y}{L}\right) , \tag{50a}$$

$$K_V S_z = F_0 \cos \frac{\pi y}{L} , \tag{50b}$$

no-flux conditions at the basin walls and defining

$$\kappa \equiv \frac{\pi}{L} \left(\frac{K_H}{K_V} \right)^{1/2} , \tag{51}$$

the steady-state solutions are given by

$$T = T_0 \cdot \left(1 + \cos\left(\frac{\pi y}{L}\right) \cdot \frac{\cosh \kappa(z+H)}{\cosh \kappa H}\right) , \tag{52a}$$

$$S = S_0 + \frac{F_0}{\kappa K_V} \cdot \cos\left(\frac{\pi y}{L}\right) \cdot \frac{\cosh \kappa(z+H)}{\sinh \kappa H} . \tag{52b}$$

For $K_H = 10^3 m^2 s^{-1}$, $K_V = 0.4 \cdot 10^{-4} m^2 s^{-1}$, $L = 10^7 m$ and $H = 5 \cdot 10^3 m$ the vertical decay scale $1/\kappa$ is about 400 m. Also, $\kappa H \approx 5$ and below mid-depth the temperature and salinity are nearly uniform and close to the average surface values T_0 and S_0. For the linear equation of state

$$\rho = \rho_0 \cdot \left(1 - \alpha(T - T_0) + \beta(S - S_0)\right) \tag{53}$$

the criterion for stability of this diffusive equilibrium is

$$\alpha T_z > \beta S_z , \tag{54}$$

which becomes, using (59),

$$\begin{aligned} R &> 1 \quad , \quad \text{for} \quad 0 < y < L/2 \quad , \\ R &< 1 \quad , \quad \text{for} \quad L/2 < y < L \quad , \end{aligned} \tag{55}$$

where

$$R = \frac{\pi \, (K_V K_H)^{1/2} \alpha \, T_0}{L \, \beta \, F_0} \quad . \tag{56}$$

Instability is therefore *inevitable* and occurs either at low latitudes ($R < 1$) or at high latitudes ($R > 1$). The solution (52) will thus never be realized. Note that R is simply the ratio of the surface buoyancy fluxes associated with temperature ($\sim \alpha\kappa K_V T_0$) and with salinity ($\sim \beta F_0$). The condition (55) states that the stabilizing effect of temperature (salinity) must dominate at low (high) latitudes for the density stratification to remain stable.

The evolution following the initiation of convective instability is different for these two cases. For the case $R < 1$, low latitude convection reduces both salinity and temperature at the surface with the reverse but weaker effects at depth. The strong feedback on temperature quickly removes the surface temperature anomaly leaving a stable stratification due to the reduced surface salinity. The system subsequently evolves again towards the unstable state and the process repeats on a time scale governed primarily by surface exchange and diffusive processes. In this case, convective mixing represents a relatively minor modification to the diffusive equilibrium.

A high latitude convective instability, on the other hand, evolves differently as observed in the experiments above and earlier by Marotzke (1989). Again, temperature anomalies are efficiently removed under the restoring conditions. Surface salinity, however, is increased by convection yielding an even less stable situation. This accelerates vertical mixing bringing warmer waters up to the surface. As a consequence of the restoring

condition on temperature heat is lost in high latitudes at an unrealistically large rate. The cooling causes a rapid increase of the density starting the violent overturning of Fig. 7c. Initially, only the high latitude density is affected so the circulation is confined to this region. However, relatively saline water is carried into adjacent surface regions triggering instability there also. The combination of very strong advection and subsequent convection homogenizes the northern half of the domain from top to bottom over a period of order two years. This rapid evolution is retarded in the southern half of the domain where the importation of deep water to the surface layer actually reduces the surface salinity hence increasing the vertical stability of the water column. The influence of the dramatic changes occuring at higher latitudes is nevertheless communicated to the equatorial region through the slower process of horizontal diffusion.

The model clearly exhibits both forms of instability. Fig. 8 shows a close-up of the evolution of the maximum and minimum streamfunction and the basin integrated surface heat flux (in PW) during the diffusion dominated state between the two flushes. Low latitude instability sets in at t = 39,500 yr evident in the surface heat flux which oscillates over the next 12,000 yr. Transport is only slightly reduced due to low latitude convection. Repeated low latitude convection and diffusion slowly increases the deep ocean temperatures thus shifting the system towards a high latitude instability. At about 52,300 yr the evolution becomes even more chaotic reducing the transport further, and eventually the high latitude instability occurs as a flush. The maximum streamfunction amplitude reaches about 400 Sv indicating the major rearrangements discussed above. We conclude that low latitude convection operating over long time scales can trigger a high

latitude instability.

5.3 Global basin

Two experiments investigating the model behaviour in one global basin are presented in this section. In the first experiment we start from the steady state 2-cell circulation of Fig. 3a, mixed boundary conditions are applied, and a weak negative salinity anomaly of 0.2 ppt is added north of 36°N as well as south of 36°S. The circulation collapses in both hemispheres each of which exhibits fields as displayed in Fig 7a. The response to the anomaly is identical to two hemispheres back-to-back with an equatorial wall. For about 3800 years no changes are apparent. From about t = 8800 yr to t= 11,800 yr small, symmetric deviations with amplitudes of order 0.5 Sv or less in transport are evident and at t ≅ 11,800 yr major transient adjustments begin. By t =13,500 yr (8500 yr after the initial perturbation) the new state consists of a single, shallow cell of 4 Sv located slightly off the equator (Fig. 9a). The subsequent evolution of this transient state is discussed below.

In the second experiment we start from the stable steady state given in Fig. 4 (reflected about the equator) and add a 2 ppt negative salinity anomaly north of 36°N only. The anomaly immediately causes a shallowing of the 1-cell circulation, and the transient state of the first experiment is obtained (Fig. 9a). During the next 22,000yr diffusion dominates and, as in the hemispheric experiment, low latitude convection occurs and causes vertical isopycnals near s = 0.4 in Fig. 9a,b. Due to vertical diffusion the deep ocean temperature has increased from 2°C to 16°C, and the water column stability has weakened accordingly. The circulation is now stronger and deeper (Fig. 9b). A few years later convection starts at high northern

latitudes and a flush begins. As in the hemispheric case a single pole-to-pole cell developes with a maximum transport of ~ 360 Sv. Heat is released at a rate of ~ 450 Wm^{-2} in high northern latitudes producing cold water that is mixed down to the deep ocean. At the same time, warm bottom water upwells in the southern hemisphere increasing the heat flux into the atmosphere. This heat loss initiates convection at high southern latitudes and also a negative circulation develops (Fig 9c). The transition passes a nearly symmetric state, and both cells then decay over the next hundred years. The southern cell eventually disappears, and the the *stable* 1-cell circulation developes (Fig. 4, reflected about s=0). Unlike in the hemispheric basin, where the several successions of flushes and collapsed states were observed, no further evolution of the 1-cell circulation was found in the global basin.

6. Concluding remarks

Several experiments in both hemispherical and a global ocean basins have been performed with the present zonally averaged ocean model. The results of MWW and Marotzke (1989) were generally confirmed. In the geometry of a hemisphere the steady states under restoring and mixed boundary conditions were found to be quantitatively similar. For surface forcing of the form (38), deep water is formed in high latitudes and upwelling occurs at the equator. When switched to mixed surface boundary conditions only minor adjustments happen; the state is stable to small perturbations. The meridional flow feeding the region of deep water formation in the present model is surface trapped. This also compares favourably with the zonal averages of 3-dimensional OGCMs (Bryan, 1986; Marotzke, 1989; Weaver & Sarachik, 1990a).

The 2-cell thermohaline circulation obtained under the restoring boun-

dary conditions is, as expected, not stable upon a switch to mixed boundary conditions. A spontaneous transition to a 1-cell circulation has already occurred by 100 years after the switch. This time is considerably shorter than the one reported by MWW but additional results show that it is strongly parameter sensitive. Application of negative or positive salinity anomalies only affects the timing of the transition phase as different feedback mechanisms are operating (Bryan, 1986). The resulting steady state is identical for the three cases. The important point is that the symmetric circulation is unstable and is not expected to occur in reality.

Long time integrations over many tens of thousands of years were performed for both hemispheric and global basins. In the hemisphere, a negative anomaly causes a break-down of the deep circulation changing it to a weak, surface trapped circulation. The deep ocean is increasingly diffusion dominated. As a result of a steady influx of heat through the ocean surface, stability of the high-latitude water column is gradually lost. After about 22,000 yr violent convective overturning sets in, and the accumulated heat in the ocean is rapidly released at rates exceeding 400 Wm^{-2} in high latitudes. A strong, basin wide circulation prevails for several hundred years only to collapse once again. This cycle was observed 3 times and is assumed to be a persistent pattern. Therefore, in the hemispheric basin at least two different modes of circulation under identical forcing could be realized.

Considering the purely diffusive steady state under mixed boundary conditions, we demonstrated that instability is inevitable and can occur either in low or in high latitudes. In the two cases the development is different, in that low latitude convective mixing has no short term basin wide effect, whereas high latitude convective mixing may trigger rapid adjustments in the

entire basin.

In a global basin the long term behaviour is different. Cycles of collapsed states and violent convective overturning do not occur. Salinity anomalies caused a collapsed circulation consisting of a weak surface trapped cell located around the equator. The deep ocean is again diffusion dominated and after about 22,000 yr convective overturning started. A few hundred years later, the stable 1-cell circulation was re-established. No further evolution of this state is expected.

With these experiments we have explored the basic dynamics and processes that occur in a 2-dimensional, zonally averaged ocean model. Some of these features were already reported by MWW and Marotzke (1989). Very similar behaviour is present in 3-dimensional ocean general circulation models, that are driven by mixed boundary conditions. In particular, Marotzke (1989) has demostrated the convective events in a hemisphere version, while Weaver & Sarachik (1990b,c) show a number of these events in both their hemispheric and global versions. The latter study finds, after many thousands of years of strong variability (episodic and cyclic), a surprisingly steady state with a zonal structure similar to that shown in Fig. 4.

The results presented here indicate that our zonally averaged model does capture the fundamental dynamics governing the meridional circulation and the associated north-south transports of heat and salt. Even in the present simple form a study of parameter sensitivities would be of interest. Unexpected responses are almost certain to be found; these could be examined in the context of the simple 2-dimensional model and then verified using an OGCM.

The results also suggest some weaknesses of the model. Specification of fixed relaxation temperatures and time scales can clearly lead to unreal-

istic effects on the meridional circulation. In particular, the strong convective events, during which the ocean loses much of its accumulated heat in a short time, would be damped by an atmosphere which communicates with the ocean surface. This heat warms the overlying atmosphere decreasing in turn air-sea temperature differences and the associated heat flux. This negative feedback is not included in ocean-only models. It is therefore a worthwile task to develop a reasonable atmosphere model that will enable us to replace the unrealistic temperature restoring boundary condition. This work is in progress (Stocker *et al.*, 1990).

The experiments have also verified that high-latitude processes are critical to the determination of the global meridional circulation. In the present study the cryosphere is absent. Inclusion of an active high-latitude ice cover would be an important extension. Ice influences both temperature and salinity. The vertical heat flux is reduced in the presence of an ice cover, resulting in a negative feedback for the ice growth. On the other hand, melting ice represents a fresh water flux which could slow down the thermohaline circulation. As a consequence, less heat is carried to high latitudes through the ocean. This, in turn, is a positive feedback for ice growth. The interaction of these two different processes could cause some interesting dynamics of the coupled ocean-ice-atmosphere system.

The present paper emphasizes the significance of the thermohaline circulation of the ocean for natural variability of the climate system and climate change. The eventual goal is to combine the present model with 2-dimensional models of the atmosphere and the cryosphere in order to obtain a realistic and yet inexpensive model suitable for paleoclimatic studies.

Acknowledgements:

The fellowship 82.613.0.88 of the Swiss National Science Foundation awarded to TFS made this study possible. This work was also partly supported

by research grants from the Canadian Natural Sciences and Engineering Research Council and Atmospheric Environment Service awarded to L.A.Mysak. We enjoyed discussions with Drs. L.A. Mysak and A.J. Weaver and thank the latter for making his OGCM data available to us.

References:

Bonsell J.J., 1988, Modelling heat fluxes in the ocean. Ph.D. thesis, St. Cross College, Trinity. 241p.

Bryan F., 1986, High-latitude salinity effects and interhemispheric thermohaline circulations. *Nature*, **323**, 301-304.

Bryan F., 1987, Parameter sensitivity of primitive equation ocean general circulation models. *J. Phys. Oceanogr.*, **17**, 970-985.

Csanady G.T., 1976, Mean circulation in shallow seas. *J. Geophys. Res.*, **81**, 5389-5399.

Fiadeiro M.E., G. Veronis, 1977, On weighted-mean schemes for the finite-difference approximation to the advection-diffusion equation. *Tellus*, **29**, 512-522.

Gill A.E., 1982, *Atmosphere-Ocean Dynamics*. Int. Geophys. Ser., **30**, 662 pp.

Gordon A.L., 1986, Interocean exchange of thermocline water. *J. Geophys. Res.*, **91**, 5037-5046.

Källén E., X.-Y. Huang, 1987, A simple model for large-scale thermohaline convection. *Dyn. Atmosph. Oceans*, **11**, 153-173.

Killworth P.D., 1985, A two-level wind and buoyancy driven thermocline model. *J. Phys. Oceanogr.*, **15**, 1414-1432.

Manabe S., R.J. Stouffer, 1988, Two stable equilibria of a coupled ocean-atmosphere model. *J. Climate*, **1**, 841-866.

Marotzke J., 1989, Instabilities and steady states of the thermohaline circulation. In *Ocean circulation models: combining data and dynamics*, D.L.T. Anderson and J. Willebrand (eds.), Kluwer, 501-511.

Marotzke J., P. Welander, J. Willebrand, 1988, Instability and multiple equilibria in a meridional-plane model of the thermohaline circulation. *Tellus*, **40A**, 162-172.

Meehl G.A., W.M. Washington and A.J. Semtner, 1982, Experiments with a global ocean model driven by observed atmospheric forcing. *J. Phys. Oceanogr.*, **12**, 301-312.

Rooth C., 1982, Hydrology and ocean circulation, *Prog. Oceanog.*, **11**, 131-149.

Stocker T.F., D.G. Wright, 1990, A zonally averaged ocean model for the thermohaline circulation. Part II: Interocean circulation in the Pacific-Atlantic basin system. *J. Phys. Oceanogr.*, (submitted).

Stocker T.F., D.G. Wright, L.A. Mysak, 1990, Experiments with a coupled, zonally averaged atmosphere-ocean model: variability of the

thermohaline circulation. *Centre for Climate and Global Change Research Report*, **90-4**, McGill University.

Stommel H., 1961, Thermohaline convection with two stable regimes of flow. *Tellus*, **13**, 224-230.

Weaver A.J., E.S. Sarachik, 1990a, On the importance of vertical resolution in certain ocean general circulation models. *J. Phys. Oceanography*, **20**, 600-609.

Weaver A.J., E.S. Sarachik, 1990b, The role of mixed boundary conditions in numerical models of the ocean's climate. *J. Phys. Oceanography.*, (submitted).

Weaver A.J., E.S. Sarachik, 1990c, Evidence for decadal variability in an ocean general circulation model: an advective mechanism. *Atmosphere-Ocean*, (submitted).

Welander P., 1986, Thermohaline effects in the ocean circulation and related simple models. In *Large-scale Transport Processes in Oceans and Atmosphere*, J. Willebrand and D.L.T. Anderson (eds.), Reidel, 163-200.

Wright D.G., J.W. Loder, 1985, A depth-dependent study of the topographic rectification of tidal currents. *Geophys. Astrophys. Fluid Dyn.*, 31, 169-220.

Tables:

Table 1: Basic model parameters

Parameter	Hemispheric	Global
ϕ_0	0°	80°S
ϕ_1	80°N	80°N
H	5000m	5000m
$\Delta\Lambda$	60°	60°
M	10	21
N	20	20
K_V	$0.4 \cdot 10^{-4} m^2 s^{-1}$	$0.4 \cdot 10^{-4} m^2 s^{-1}$
K_H	$10^3 m^2 s^{-1}$	$10^3 m^2 s^{-1}$
A	$10^{-4} m^2 s^{-1}$	$10^{-4} m^2 s^{-1}$

Figure Captions:

Figure 1: The relation between the left and right hand sides of (47a) determined from the steady state circulation of the Bryan-Cox OGCM in a hemispheric basin with no wind stress (Weaver & Sarachik, 1990a,b). The values are plotted for 27 latitudes from 60°S to 5°S at depth 570m (×) and 2135m (+); scales are multiplied by 10^{-3}. The slopes and correlations are -0.163, -0.785 for (×) and -0.182, -0.866 for (+).

Figure 2: Constant of proportionality ϵ and correlation of the linear fit as functions of depth. Correlations are exceeding 0.9 for the main part of the water column; ϵ increases over the first 500m and is nearly constant at $\epsilon \approx 0.2$ below.

Figure 3: Contours of the meridional overturning streamfunction in Sv (1 Sv = $10^6 m^3 s^{-1}$), (a), and density anomaly in kgm^{-3}, (b). The steady state in a global basin under restoring boundary conditions consists of 2 cells with deep water formation in both high latitudes. Meridional heat flux (dotted) in PW (1 PW = 10^{15} W) and vertical surface heat flux (solid) in Wm^{-2}, (c) are symmetric about the equator. The vertical surface salt flux is given as an equivalent fresh water flux E-P in m/yr, (d).

Figure 4: Contours of the meridional overturning streamfunction, (a), and density anomaly, (b), of the steady state of Exp. I under mixed boundary condition at t=7400 yr.

Figure 5: Steady state overturning streamfunction for a hemispheric basin under restoring boundary conditions (a, t=5050 yr) and mixed boundary conditions (b, t=10,000 yr). The change in condition type causes only minor adjustments.

Figure 6: Time series of the maximum streamfunction during 80,000 yr of integration in a hemispheric basin after a positive salt anomaly of 0.1 ppt north of 36°N. Three *flushes* occuring about every 22,000 yr are observed.

Figure 7: Overturning streamfunction and density anomaly at different times in Fig. 7: t=8000 yr (a), t=28,610 yr (b), t=28,620 yr (c). The states of (a) and (b) are diffusion dominated leading to the violent overturning (flush, >300 Sv) in (c).

Figure 8: Analysis of the evolution between the first two flushes of Fig. 6 (a). Maximum and minimum streamfunction (solid) and total surface heat flux (dotted) evolve smoothly for about 9000 yr after the first flush (b), when low latitude instability sets in at t=39,500 yr. This leads eventually to larger perturbations (t=52,500 yr) which trigger the high latitude instability causing the flush at t=53,850 yr, (c).

Figure 9a: Evolution of the deep circulation in a global model after

adding fresh water in both high latitudes to the state of Fig. 3a or, alternatively, adding fresh water only to the high northern latitudes of Fig. 4 (reflected about the equator). Both perturbations lead to the collapsed state.

Figure 9b: Evolution of the collapsed circulation of Fig. 9a. The equatorial cell deepens over the next 22,000 years. The state at t=31,660 yr is just before a flush.

Figure 9c: Violent convective overturning starts with a northern cell first, a southern cell is set up later; t=31,705 yr.

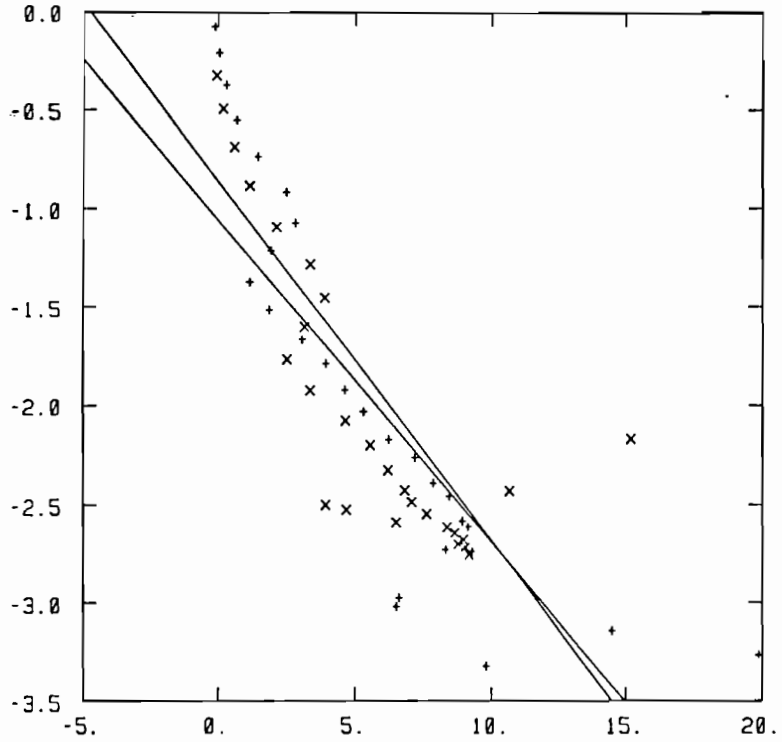

$\frac{\Delta(p-p_s)}{\Delta\Lambda}$

$\sin 2\phi \ \frac{\partial(p-p_s)}{\partial\psi}$

Fig 1

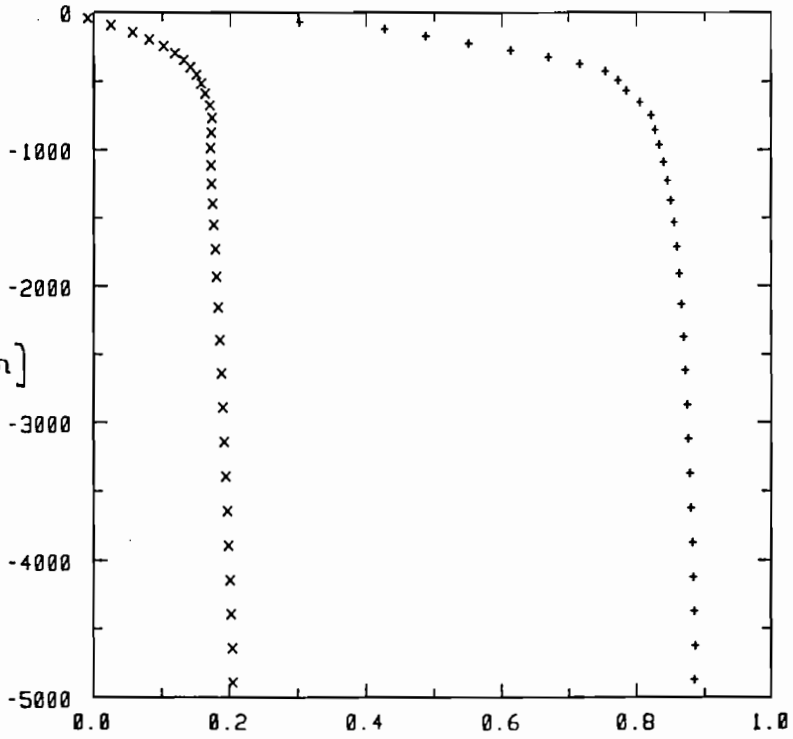

z [m]

ε , r

Fig 2

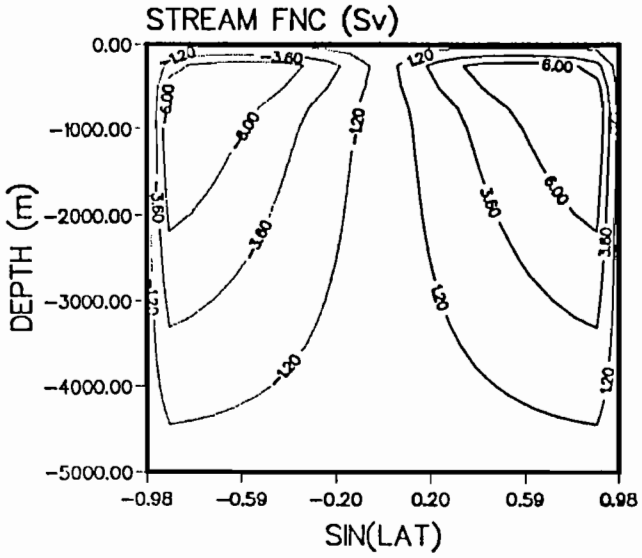

Fig 3a

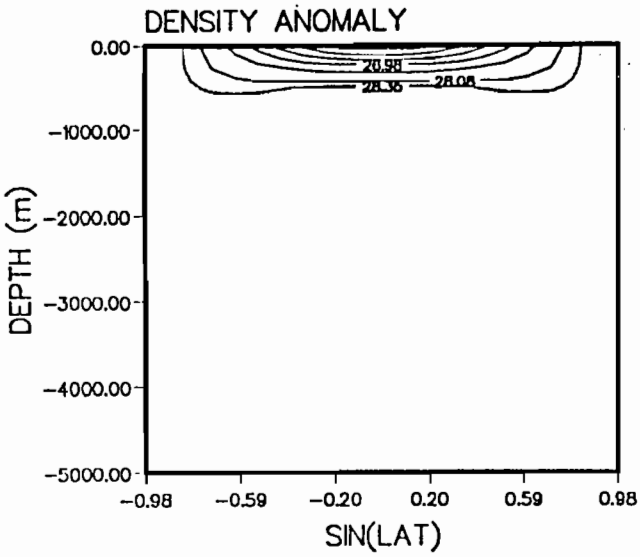

Fig 3b

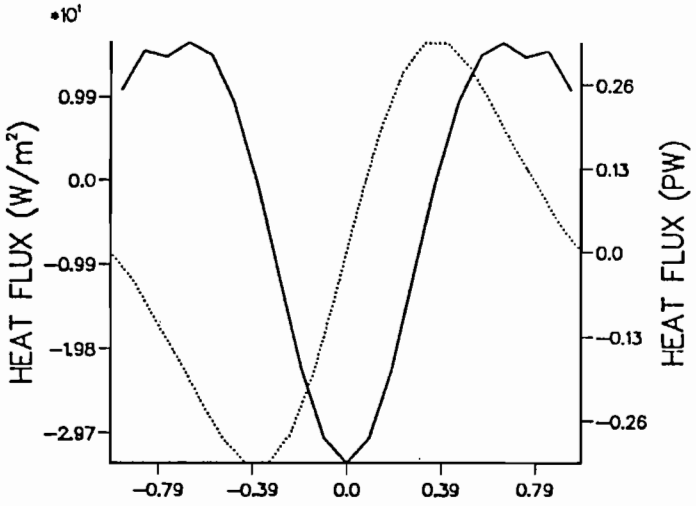

fig 3c

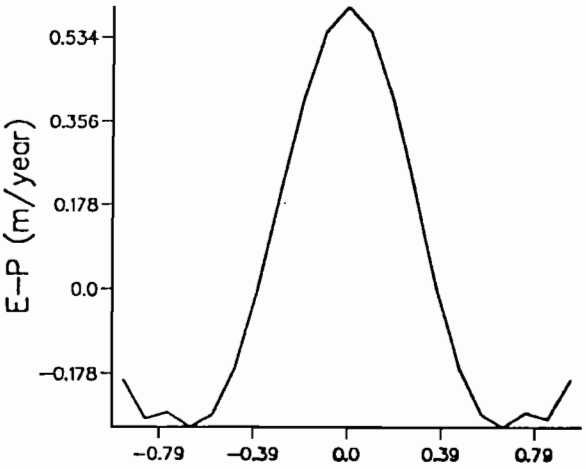

Fig 3d

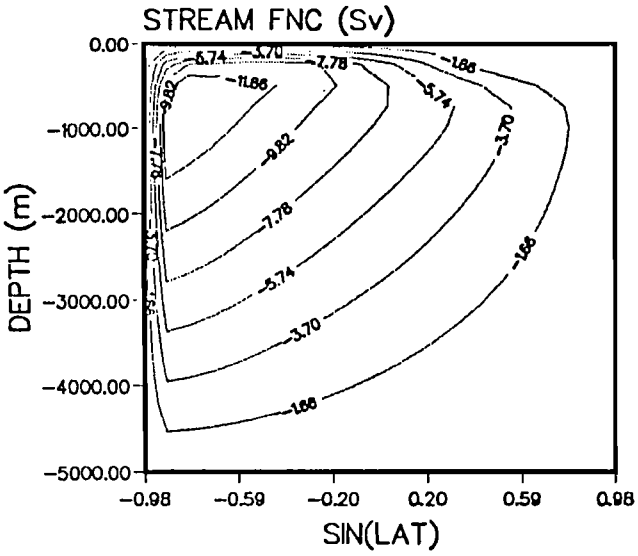

Fig 4a

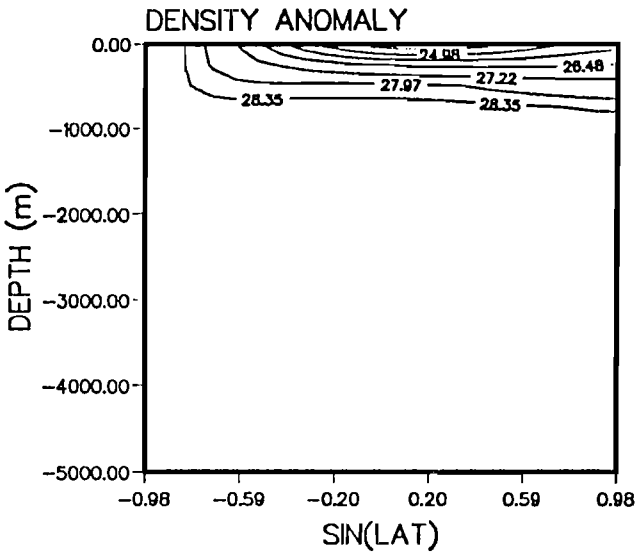

Fig 4b

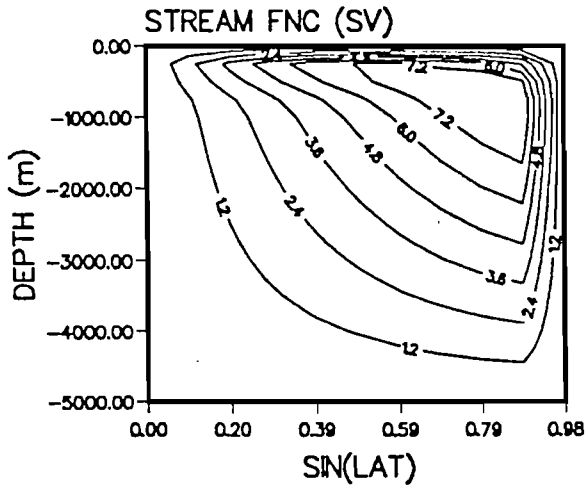

Fig 5a

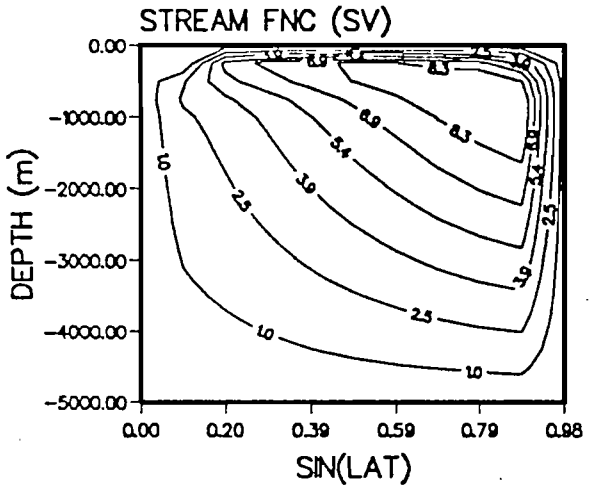

Fig 5b

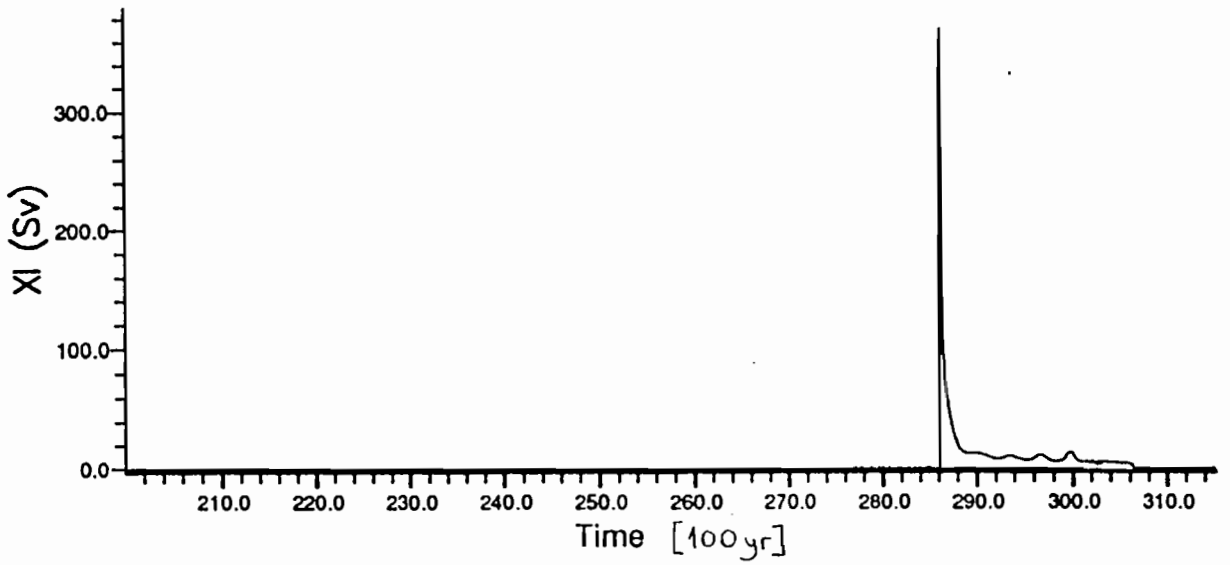
300.0
200.0
100.0
0.0
XI (Sv)
210.0
220.0
230.0
240.0
250.0
260.0
270.0
280.0
290.0
300.0
310.0
Time [100yr]

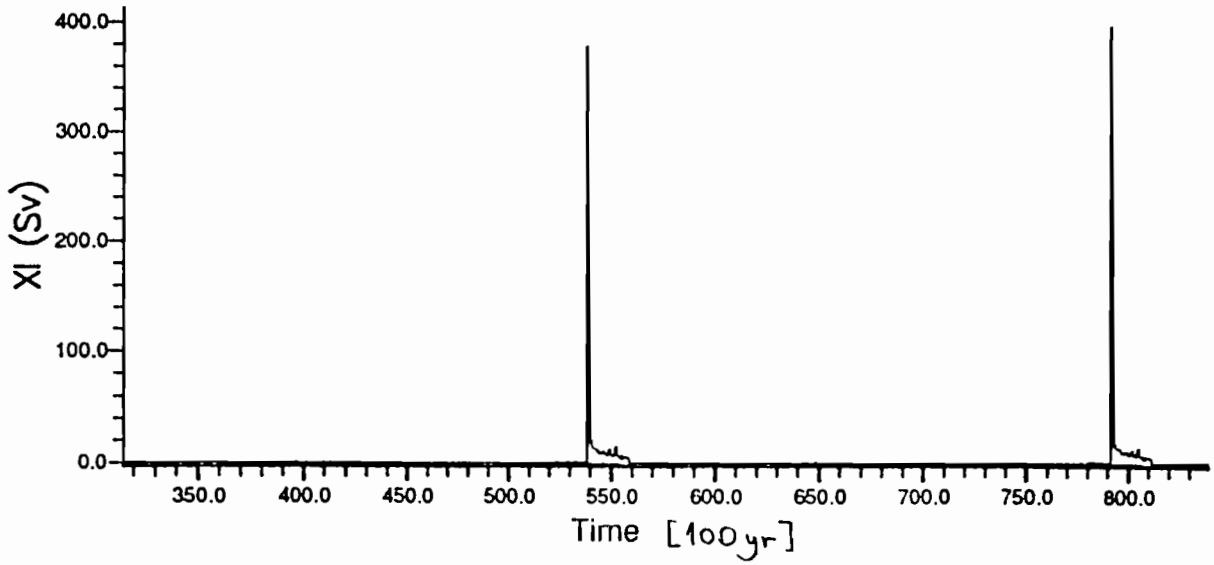
400.0
300.0
200.0
100.0
0.0
XI (Sv)
350.0
400.0
450.0
500.0
550.0
600.0
650.0
700.0
750.0
800.0
Time [100yr]

Fig 6

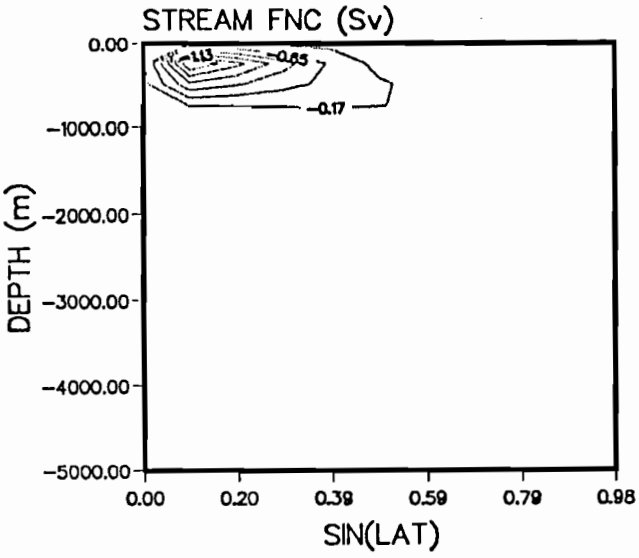

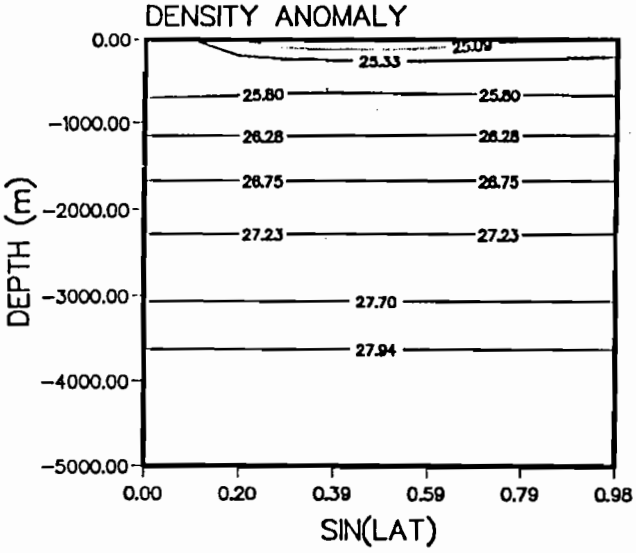

Fig 7a

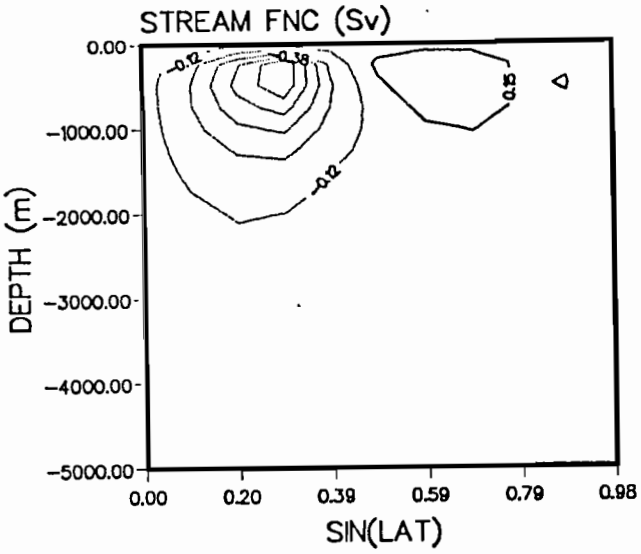

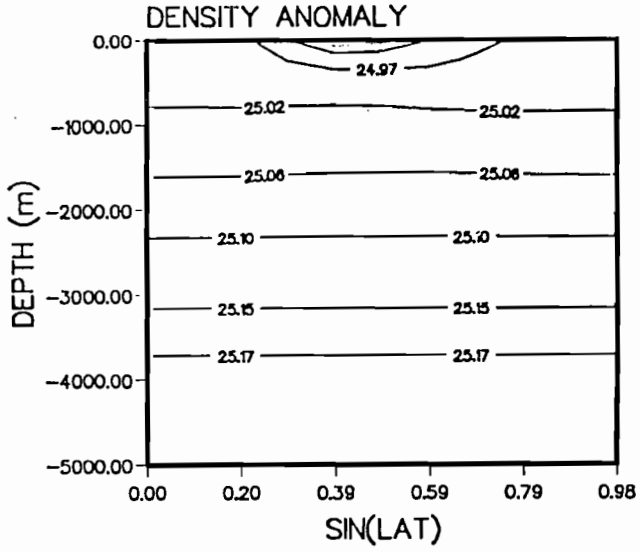

Fig 7b

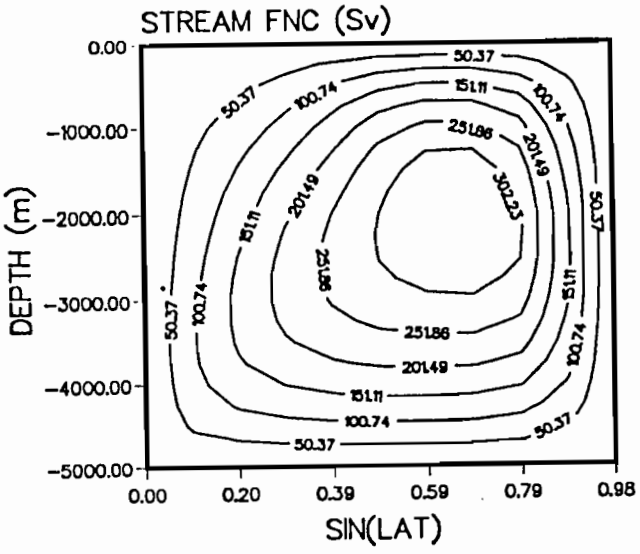

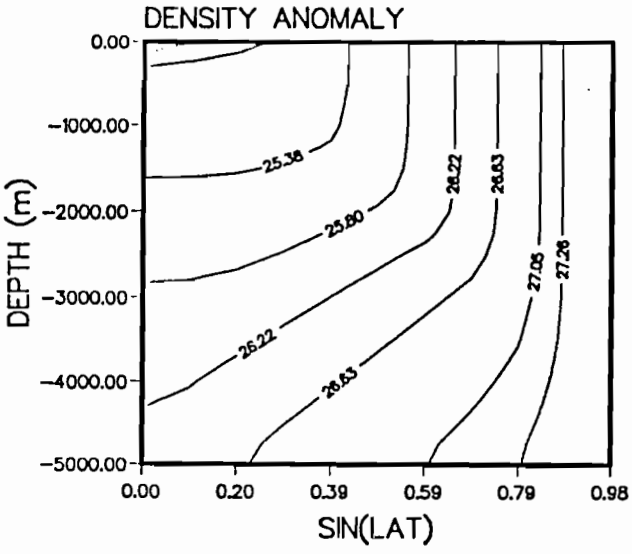

Fig 7c

Fig 8a

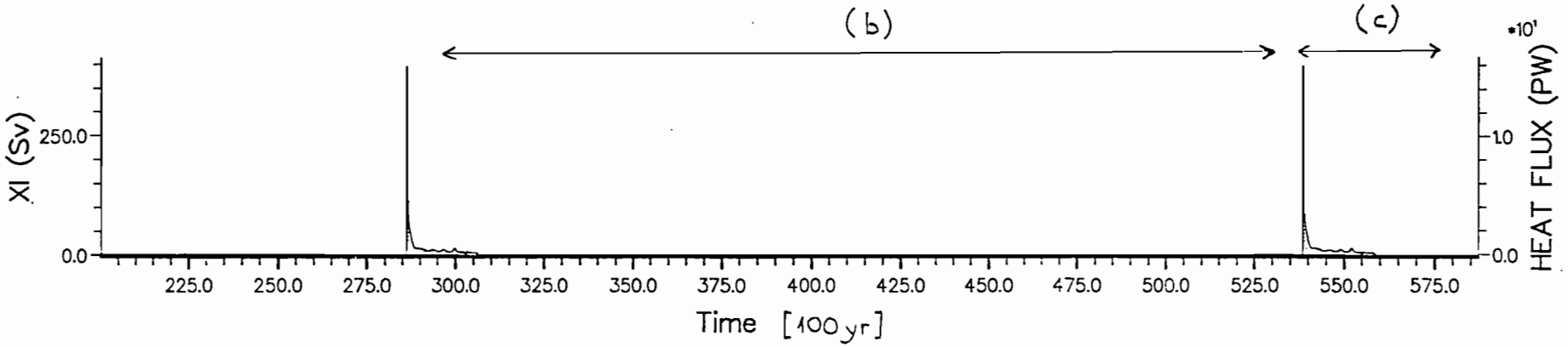

Fig 8b

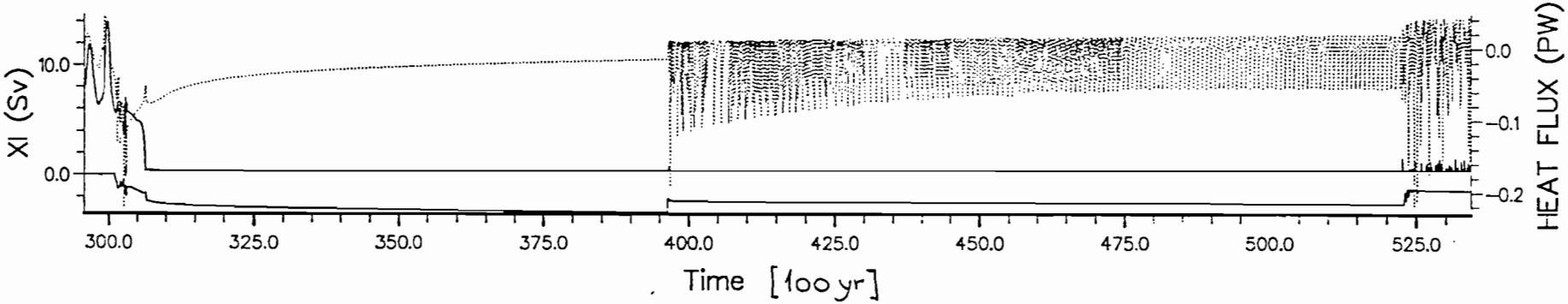

Fig 8c

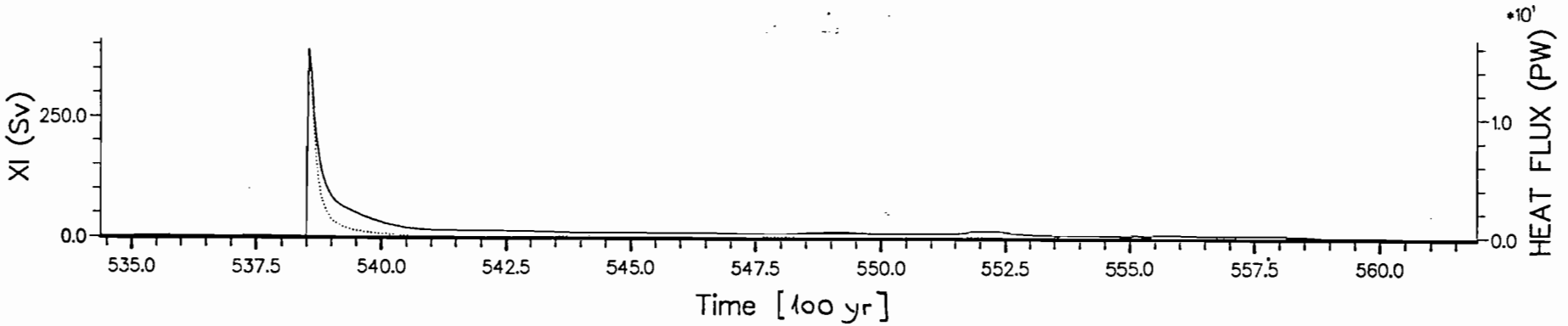

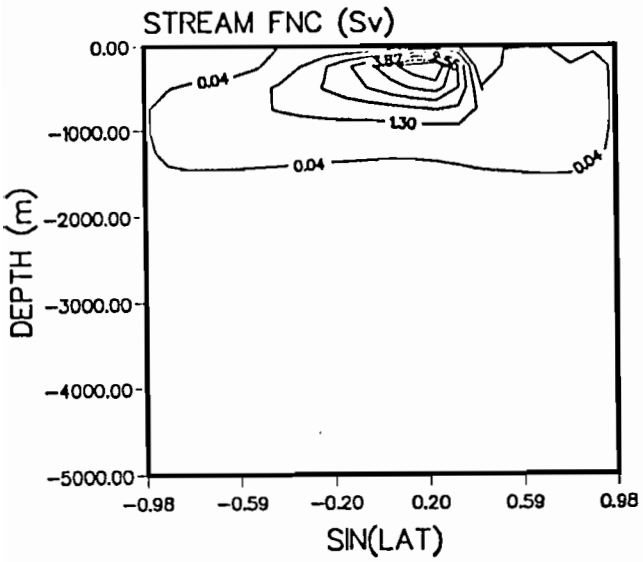

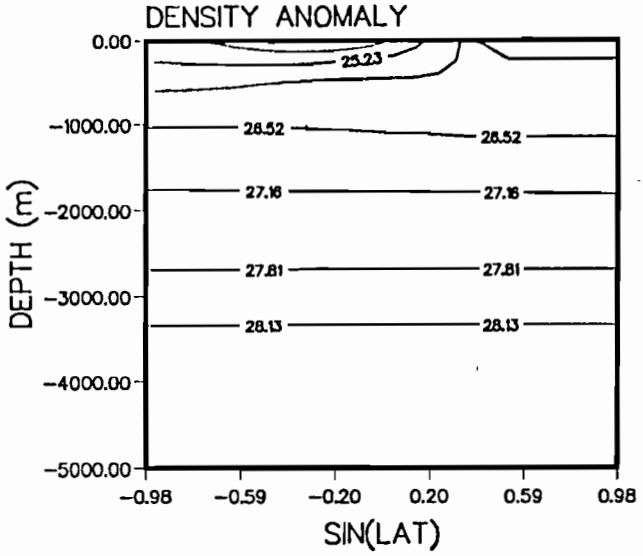

Fig 9a

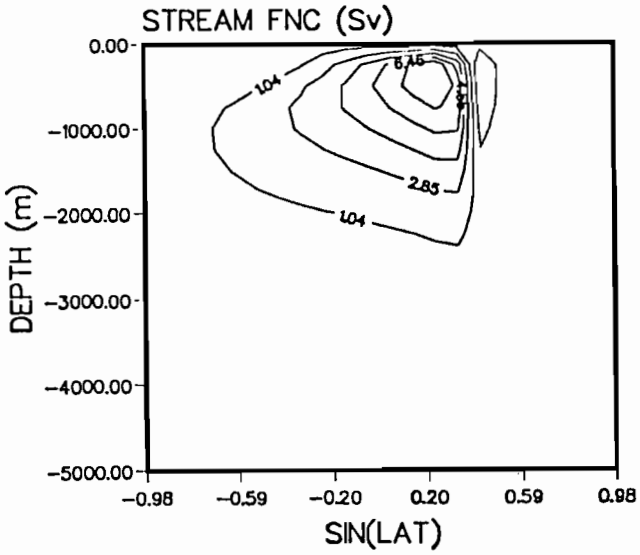

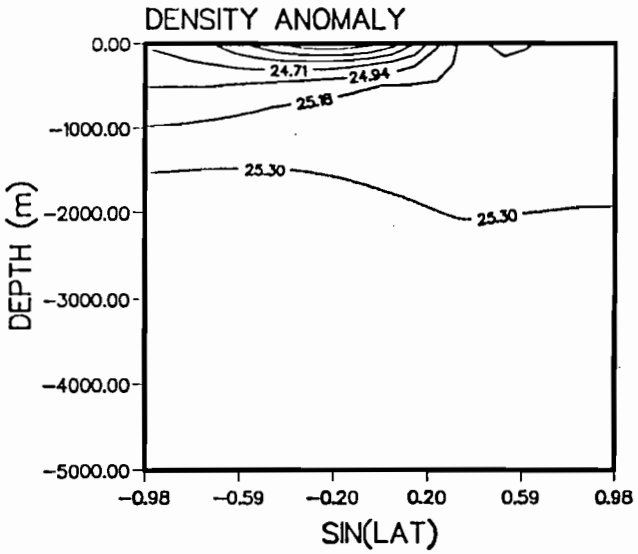

Fig 9b

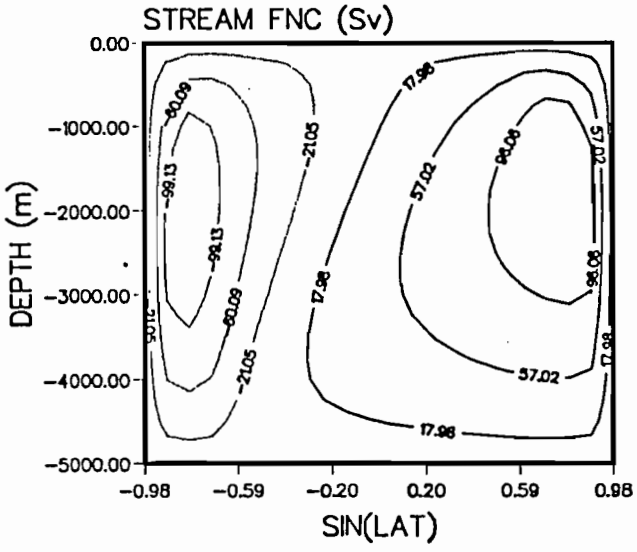

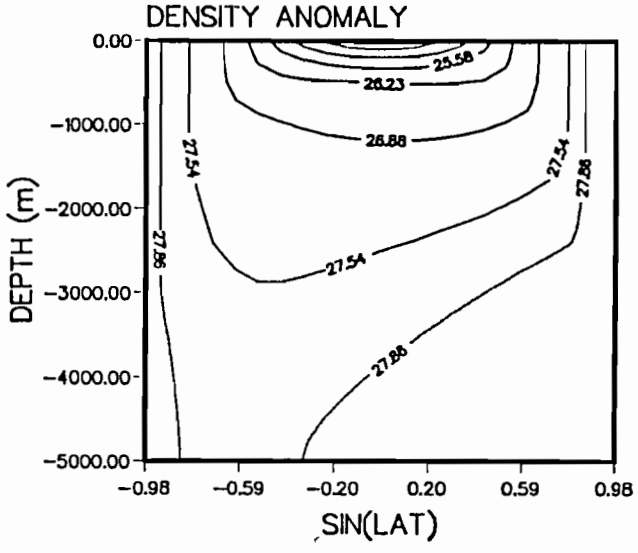

Fig 9c

A Zonally Averaged Ocean Model for the Thermohaline Circulation.

Part II: Interocean Circulation in the Pacific-Atlantic Basin System

Thomas F. Stocker & Daniel G. Wright*

C^2GCR Report No. 90-13
September 1990

submitted to

Journal of Physical Oceanography

September 1990

Abstract

The zonally averaged, latitude-depth ocean model developed in Part I (Wright & Stocker, 1990) is extended to a 2-basin system representing the Atlantic and Pacific. Steady states are calculated under two different surface boundary conditions to study a possible global thermohaline circulation linking the Pacific and the Atlantic (Gordon, 1986). If the surface temperature and profiles are identical functions of latitude in both Pacific and Atlantic, the steady state under restoring boundary conditions exhibits, inspite of the different basin extensions, the familiar 2-cell structure in both basins. Upon switching to mixed boundary conditions the state is unstable, and a 1-cell circulation with downwelling at high northern latitudes develops in each basin.

For a realistic surface salinity profile that is fresher in the Pacific, the steady state under restoring boundary conditions is completely different. It exhibits a global thermohaline circulation with strong interocean mass exchange. Deep water is formed primarily in the North Atlantic from which a deep flow spreads into the Pacific, where it upwells. This state is stable also under mixed boundary conditions. The meridional heat flux is to the south in the Pacific and to the north in the Atlantic with maximum values of order 0.7 PW (1 PW = 10^{15}W). Both temperature and salinity structures of the steady state compare favourably with the zonal averages of Levitus (1982). The model also demonstrates that this interocean thermohaline circulation is maintained by net evaporation in the Atlantic and net precipitation in the Pacific.

A deglaciation experiment is performed by applying a fresh water flux anomaly in the North Atlantic. A flux representing the conditions during the

ice melt at the last ice age termination reverses the thermohaline circulation in the Atlantic resulting in a meridional heat transport to the south. For half the anomaly the interocean circulation remains stable but with weaker deep water formation in the North Atlantic. The global thermohaline circulation thus exhibits more than one stable equilibrium under realistic surface forcing.

1. Introduction

Beyond controlling the meridional heat flux in a single ocean basin like the Atlantic, the thermohaline circulation is likely to have a global significance within the climate system. Observations confirm that the main region of deep water formation is located in the North Atlantic (Warren, 1981) with rates estimated at 14 to 20 Sv (1 Sv = $10^6 m^3 s^{-1}$), while the Pacific Ocean shows primarily upwelling. Based on an analysis of water characteristics in the main ocean basins, Gordon (1986) proposed that these two areas are linked by a thermocline flow of relatively warm water from the Pacific through the Indian Ocean into the South Atlantic thus feeding deep water formation in the North Atlantic. A corresponding Atlantic deep water flow is exported to the Indian and Pacific Oceans via the Antarctic Circumpolar Current (ACC). Such a global thermohaline circulation would connect the three major ocean basins acting like a conveyor belt for water masses and would represent a key element of our climate system.

In Part I (Wright & Stocker, 1990) we have developed a zonally averaged ocean model and shown qualitative agreement with 3-dimensional ocean general circulation models (OGCMs). We are therefore encouraged to apply an extended version of the model to investigate whether the main ocean basins are indeed connected by a global thermohaline circulation (Gordon, 1986). A second

purpose of this paper is to study the stability of such a conveyor belt circulation. More specifically, how does a fresh water flux released into the Atlantic Ocean during the termination of an ice age affect the global thermohaline circulation ?

Support for the idea that the various ocean basins are communicating via a thermohaline flow was recently provided by at least two 3-dimensional OCGM experiments. Cox (1989) studied the water mass structure of the world ocean steady state under zonally uniform restoring boundary conditions on both temperature and salinity. When the thermohaline flow was enhanced by adding salt to the North Atlantic, water masses originating from the North Atlantic were identified in the Indian and Pacific ocean. Maier-Reimer & Mikolajewicz (1989) presented results of the global, annual-mean version of the Hamburg OGCM which was spun up under restoring boundary conditions for 10,000 yr. From this steady state the salt flux was diagnosed, and integration continued under mixed boundary conditions. The model was able to clearly reproduce a global thermohaline circulation linking the main ocean basins. In addition, a two-basin system was investigated by Wells & Mead (1989) using the Bryan-Cox OCGM for various restoring boundary conditions and geometries. The preliminary study, however, shows unrealistically large overturning in the Atlantic (> 60 Sv), when asymmetric salinity forcing is applied, and the interbasin flow remains to be analyzed.

Variability of the thermohaline circulation can be an important factor for climatic change. Stommel (1961) pointed out that a perturbation of the ocean system could cause it to jump into a different mode of operation. The presence of stable and unstable equilibria in ocean models was confirmed by a number of recent OGCM model studies (see Part I for a discussion). Broecker *et al.* (1985) give evidence of significant changes in deep water

formation rates of the North Atlantic during the termination of the last ice age. Melt water of the disintegrating North American ice sheets, which flows into the North Atlantic at various latitudes, can influence the thermohaline circulation. The immediate local effect is to stabilize the water column and decrease deep water formation which results in a reduced oceanic meridional heat transport. If the global conveyor belt flow suggested by Gordon (1986) is operating, one must expect that a modification of the Atlantic deep circulation will also have a global impact.

The early model studies (Bryan, 1986; Marotzke *et al.*, 1988) on the effect of deglaciation on the thermohaline circulation use unrealistic scenarios and consider only one ocean basin. A steady state is perturbed by adding or removing salt at a given time. Anomalous run-off, however, does not directly affect the salinity field nor is it operating only during a very short time. More realistically, the surface flux field of salt is modified for several thousand model years. This was first done by Maier-Reimer & Mikolajewicz (1989) in their global OGCM. Their results indicate that an anomaly, that is 10 times smaller than the current estimate of about 0.1 Sv is already sufficient to switch off the Atlantic meridional heat transport.

The paper is organized as follows. Section 2 explains the model set up. The steady states that evolve under symmetric surface forcing and their stability are presented in section 3. Section 4 deals with the global thermohaline circulation obtained when realistic surface salinity is used. Two deglaciation experiments are discussed in section 5. Conclusions follow in section 6.

2. Model set-up for the Pacific-Atlantic basin system

To simulate a global thermohaline circulation, the ocean model is ex-

tended to two basins of 120° and 60° angular width representing the Pacific and Atlantic, respectively. The Pacific basin extends from 55°S to 50°N, the Atlantic from 55°S to 80°N. The Antarctic Circumpolar Current (ACC) region is modelled by a single column of grid boxes with 360° angular width. Thus, within the ACC region, neither the zonal nor the meridional structure of water mass properties are resolved. This region joins both the Pacific and the Atlantic basins through flux balances of mass, heat and salt, and represents the only oceanographic connection between the two basins.

Exchanges between the ACC region and the individual basins depend strongly on the value of ϵ relating the east-west and north-south pressure gradient components. The parametrization is explained in Part I (eq. 41), where we argued that the value of ϵ depends on the width of the basin. Here we assume that, for a specified north-south density gradient, the density contrast across a wide basin is independent of the width of the basin. Combined with the hydrostatic approximation, this suggests that the pressure difference across the basin is independent of the basin width so the pressure gradient (and hence ϵ) is inversely proportional to the basin width. This is also consistent with the fact that the zonally averaged east-west velocity comes closer to geostrophy with increasing angular width.

Various runs have shown that $\epsilon = 0.2$ for the Atlantic and $\epsilon = 0.1$ for the Pacific yield reasonable values of the meridional overturning under realistic surface forcing. The coincidence with the independent analysis of the 3-dimensional OGCM (Part I, section 2.3), which gives $\epsilon = 0.2$ for the Atlantic, is remarkable.

The numerical scheme used is essentially the same as that in Part I. Fluxes across cell boundaries are estimated using the method of Fiadeiro and Veronis (1977), and forward time differencing is applied. Calculations are

performed on three different grids labelled A, 15 (horizontal) × 10 (vertical), B, 31 × 10, and C, 31 × 20 points.

To obtain a steady state circulation the standard procedure of ocean spin-up is applied. Integration starts from an ocean at rest with uniform temperature T = 7°C and salinity S = 35 ppt. The circulation is set up by thermal and haline surface forcing. T and S at the ocean surface are relaxed to specified values T^* and S^* on a time scale $\tau_H = \tau_S = 100$ days. The following analytic forms are used initially:

$$T^*(s) = (1 + \cos(\pi s)) \cdot 12.5^{\circ}C, \qquad (1a)$$

$$S^*(s) = (36 + \cos(\pi s)) \cdot \text{ppt}\ , \qquad (1b)$$

where $s = \sin\phi$ is the sine of latitude.

Once a steady state under restoring boundary conditions is reached, the vertical salt flux is diagnosed and used henceforth as the constant surface forcing on salinity; surface temperatures are still relaxed to (1a). Further integrations are carried out under these mixed boundary conditions.

The next section presents the global thermohaline circulations obtained under symmetric surface boundary conditions for both the restoring and the mixed type.

3. Global thermohaline circulation under symmetric salinity forcing

Here, temperature and salinity are restored to symmetric forcing fields, i.e. Pacific and Atlantic latitudes have identical restoring values given by (1). Figure 1a shows the meridional overturning streamfunction after 1000 yr of spin-up under restoring boundary conditions using the coarse grid A. The resulting thermohaline circulation consists of 2 cells in each ocean basin. Deep water is formed primarily in the ACC region (10 Sv in

the Atlantic, 14 Sv in the Pacific part), in the North Atlantic (9 Sv) and a shallow cell of 6.5 Sv in the North Pacific. There is no cross-basin mass flux, and the flow shows the structure of two independent basins which are individually forced. The asymmetries between Pacific and Atlantic are due to the fact that the Pacific basin only extends to 50°N.

The salt flux in both basins was diagnosed from this state, the boundary condition was switched to the mixed type, and a 0.5 ppt positive salinity anomaly was added in the Atlantic north of 32°N. As expected, the circulation is not stable, a transition occurs and after 1000yr cross basin flow of about 4 Sv is observed (Fig 1b). Deep water formation in the ACC has ceased, and the North Pacific cell is now stronger (10 Sv). After another 1000yr of adjustment both basins have a 1-cell circulation with deep water formation in the northern latitudes only (Fig. 1c). The rates are 13 Sv and 15 Sv in the Atlantic and Pacific, respectively. Interocean exchange has almost ceased resulting in nearly independent thermohaline circulations in the two basins.

This experiment shows that the geometrical asymmetry is not sufficient to produce a steady interocean exchange of water in this model. Under steady symmetric forcing, the system evolves to a state in which the interaction between the two basins is minimal.

4. Global thermohaline circulation under realistic salinity forcing

In this section steady state circulations under restoring and mixed boundary conditions are obtained for the three grid configurations A, B and C with the vertical diffusivity $K_v = 0.4 \cdot 10^{-4}$ $m^2 s^{-1}$. The restoring profiles of T^* and S^* are given by (1a), and

$$S^*(s) = \left[35 + \cos(\pi\, s) + \frac{s_P - s_A}{s_P + s_A} + \begin{cases} + \Delta S \dfrac{s - s_{0A}}{s_P + s_A} \Big] \cdot \text{ppt}\,, & \text{Atlantic} \\ - \Delta S \dfrac{s - s_{0P}}{s_P + s_A} \Big] \cdot \text{ppt}\,, & \text{Pacific} \end{cases} \right. \tag{2}$$

where s_{0A}, s_{0P}, s_{1A}, and s_{1P} are the sines of the latitudes of the southern and northern extents of Atlantic and Pacific basins, respectively, and $s_P = s_{1P} - s_{0P}$, $s_A = s_{1A} - s_{0A}$. Superposed on the restoring salinity given by (1) is therefore a linear variation with an increase of about $\Delta S \cdot$ppt from the North Pacific through the ACC to the North Atlantic. We select $\Delta S = 2$ corresponding to realistic conditions, unless stated otherwise. Figure 2 shows the surface temperature (a, solid) and salinity (b, solid) for the steady state on grid A obtained after 7000yr of integration. The profiles are compared to the zonal averages (dashed) of Levitus (1982). Note that the equatorial salinity minima are not included in (2) and hence not present in the surface salinity field.

Due to the asymmetric salt forcing (2), the ocean spin-up takes much longer to reach steady state. Since the vertical surface salt flux integrated over both basins must vanish for a steady state, this quantity is a useful indicator of deviations from equilibrium. After 7000 years of spin-up under restoring boundary conditions the integrated salt flux is 4 orders of magnitude smaller than typical values in each basin. Decreasing vertical heat and salt fluxes integrated over both basins are given in Tab. 1.

Figure 3a displays the meridional overturning streamfunction on grid A in the two ocean basins after 7000 years under restoring boundary conditions (1a) and (2). The state is essentially steady. Deep water is formed at a rate of 16 Sv *in the North Atlantic only*. The Atlantic bottom water flows south, and about 7 Sv are exported into the Pacific. The rest is upwelling

in the Atlantic and joins the thermocline return flow from the Pacific. In the Pacific about 10 Sv are upwelling, the main part of which originates from Atlantic bottom water. About 7 Sv are returned to the Atlantic as a shallow flow through the ACC (vertically dashed). An additional 4 Sv of intermediate water production occurs within the ACC being returned into the South Pacific. Two weak (4 Sv) and shallow cells in the South Atlantic and the North Pacific are also observed.

The surface fluxes of heat and salt are displayed in Fig. 2 (dash-dotted). At t=7000yr the salinity flux in both basins is diagnosed and used for further integration under mixed boundary conditions. When the integration is continue with no other changes, only small adjustments occur in the salinity field. The thermohaline circulation for t= 12,000yr is given in Fig. 3b; minor differences can be seen. We conclude therefore, that this state is *stable* against small perturbations.

To study the influence of the northward extension of the Atlantic basin two additional spin-up runs on grid A under restoring boundary conditions (1a) and (2) with $\Delta S = -2$ and $\Delta S = -4$ are performed; note that here the Atlantic is fresher than the Pacific. In the former case, $\Delta S = -2$, the circulation is similar to Fig. 1a, except that North Atlantic deep water formation is shallow (~ 5 Sv) and sinking in the North Pacific reaches about 3000m (~ 10 Sv). No interocean flow is observed. Upon switching to mixed boundary conditions, this state is again unstable, and the new equilibrum state is similar to Fig. 1c. Only for the large salinity contrast, $\Delta S = -4$, does a reversed global thermohaline develop. Therefore, in this model the present geographical extension of the Pacific and Atlantic basins favours the conveyor belt circulation as shown in Fig. 3b, but is not the cause of its maintenance. This will be discussed below.

Dependence of the flow on the grid resolution is studied next; all other parameters such as vertical diffusivity and relaxation time scales are unchanged. Spin-up under restoring boundary conditions and then switching to mixed boundary conditions is repeated independently for each grid resolution. Qualitatively similar flows are obtained when increasing the resolution. The steady state meridional overturning streamfunctions are given in Fig. 3. for grid B (Fig. 3c) at t=16,000yr (mixed boundary conditions since t=8000yr) and grid C (Fig. 3d) at t=10,000yr (mixed boundary conditions since t=8000yr). Differences are summarized in Tab. 2. The maximum transport does not vary much when the horizontal resolution is increased, however for C, with double the vertical resolution we get a reduction in the maximum transport from about 17 Sv to 12 Sv. This is a reflection of generally reduced horizontal density gradients with increased vertical resolution.

Part of this discrepancy can be directly related to the restoring surface boundary condition (Part I: eq. 18, 19a). As Δz is reduced, the relaxation time scale should also be reduced approximately in proportion. However, vertical diffusivity is also important. Because surface temperature is obtained by linear extrapolation from the two uppermost grid cells, its effective diffusivity within the top cell is infinite. This influence is greater for coarser vertical resolution. By doubling K_V and halving the relaxation time we obtain similar transports again (Tab. 2).

Before analyzing the various fields, a phenomenon, which occured at resolution B, is briefly discussed. Figure 4 shows a time series of the maximum and minimum transport for 16,100yr < t < 16,600yr. A remarkable periodic variability of the global thermohaline circulation is observed. The period is 38 years, and the fluctuations persist over 8000yr with a peak-to-peak amplitude of 1.2 Sv or about 7% . Similar variability can be inferred for

the climate relevant meridional heat transport. As a rough estimate of the climatic significance of this periodic variability consider a typical 1 Wm^{-2} change in the ocean-atmosphere heat flux. This would cause a temperature fluctuation of about 0.3°C assuming grey body radiation for the surface temperature.

Given the steady forcing, the variability is apparently a self-sustained oscillation. Therefore, even in this idealized ocean model natural variability *does* occur, indicating again that the ocean is an active component of the climate system. A similar phenomenon of decadal variability was recently found by Weaver & Sarachik (1990) in their 3-dimensional OGCM.

An additional experiment on grid B was performed with a doubled vertical diffusivity $K_V = 0.8 \cdot 10^{-4}$ $m^2 s^{-1}$ (Tab. 2). The steady state under mixed boundary conditions is qualitatively similar to Fig. 3c, however with a maximum transport of 20.2 Sv. This increase is in good agreement with the 1/3-power law between meridional transport and vertical diffusivity (Bryan, 1987). The self-sustained oscillation is absent for the increased diffusivity, and no fluctuation of the steady state is observed. A spurious numerical mode can be excluded as a cause of the variability in the previous run; one cycle of the oscillation is covered by more than 550 time steps. The result rather indicates that the vertical diffusivity is an important parameter which strongly influences the natural variability of the thermohaline circulation.

The temperature and salinity fields of the flow are now analyzed for a run with realistic salinity and temperature forcing. Restoring surface salinity is given by (2), and for the restoring surface temperature we select

$$T^*(s) = \left(14.5 + 12.5 \cdot \cos\left(\frac{\pi}{2}\, s \cdot (1+|s|)\right)\right) \cdot \text{°C} \quad , \qquad (3)$$

which is a good approximation to the data by Levitus (1982). The model is spun up under restoring boundary conditions for 6000 yr on grid C using K_V = $0.8 \cdot 10^{-4} m^2 s^{-1}$ and $\tau_S = \tau_H$ = 50 days. From this steady state the integration continues for 2000 yr under mixed boundary conditions. The meridional overturning streamfunction at t=8000 yr is shown in Fig. 5a. Deep water formation occurs only in the North Atlantic at a rate of 19 Sv; 11 Sv flows as a deep current into the Pacific basin where it upwells over a broad region. Intermediate water is formed in the North Pacific (2.6 Sv) and in the Pacific part of the ACC region (15 Sv), part of which (10 Sv) flows into the South Atlantic.

Figure 5b gives the latitude profiles of sea surface temperature (model and Levitus data) and the vertical ocean-atmosphere heat flux in Wm^{-2}. The model ocean temperature varies from 10.7°C (2.89°C) in the North Pacific (North Atlantic) to 27°C at the equator and falls to 3.97°C in the ACC region. The vertical heat flux is negative in both equatorial regions, where the ocean receives energy at rates of 12 and 20 Wm^{-2} in the Pacific and Atlantic, respectively. Most of the heat is released in the North Atlantic at an average of 30 Wm^{-2} and at somewhat less than half this rate in the South Pacific.

Sea surface salinity (model and Levitus data) and the vertical salt flux are given in Fig 5c as functions of latitude. Maximum salinities occur at the equator with 35.5 ppt in the Pacific and 36.5 ppt in the Atlantic; the North Pacific is fresh at 33.5 ppt while the North Atlantic has 35.0 ppt. The salt flux can be converted to P-E rates; the model shows a negative salt flux due to evaporation excess in the equatorial regions with -0.18 myr^{-1} and -0.49 myr^{-1} in the Pacific and Atlantic, respectively. The basin integral over the Atlantic indicates a *net evaporation excess* of -0.125 myr^{-}

^{1} (-0.058 myr^{-1} and -0.213 myr^{-1} over the North and South Atlantic, respectively) which in turn is compensated by a *net precipitation excess* over the Pacific. Baumgartner & Reichel (1975) give an observed value of -0.175 myr^{-1} (-0.122 myr^{-1} and -0.236 myr^{-1} over the North and South Atlantic, respectively). Considering the large uncertainties of these estimates the model successfully reproduces the observed water transport through the atmosphere and river run-off from the Atlantic to the Pacific.

Atmospheric freshwater transport is essential to maintain the global thermohaline circulation. This is confirmed by an experiment starting from the steady state of Fig. 3b and modifying the surface salt flux such that there is no net flux into either basin. After 1500 yr of further integration the global conveyor belt is replaced by a flow which consists of one cell in each basin with deep water formation in both southern oceans, similar to Fig. 10a (below). Thus the surface salinity contrast and different evaporation rates between Atlantic and Pacific are closely linked to interocean exchange of freshwater by the global thermohaline circulation.

The Atlantic heat flux (Fig. 5d) is mainly northward with a maximum of 0.66 PW (0.41 PW across the equator). The Pacific, on the other hand, has a heat transport to the south peaking at 0.69 PW (0.37 PW across the equator). Although a substantial interocean mass flux is evident from Fig. 5a there is very little exchange of heat between the basins.

Figure 6a presents the latitude-depth temperature field of the Pacific, which is compared to the zonal averages by Levitus (1982) (Fig. 6b). The model shows the observed stratification and the well mixed regions of the upper 1000 m of the South Pacific. As expected, the weak equatorial doming due to Ekman pumping is not present in the model.

The salinity field is given in Fig. 7a for the model and in Fig. 7b for

the Levitus (1982) data. Near the equator the model and observed salinities decrease with depth over the upper 600m, below which there is well mixed intermediate water. From the North Pacific and the South Pacific tongues of *fresh water* intrude equatorward between about 600m and 1000m. The columns adjacent to the ACC are well mixed over the upper 1000m. The deep ocean is uniformly stratified with only a very weak latitude dependence showing doming in the equatorial regions. All these features are in good agreement with the observations.

The temperature field of the Atlantic (Fig. 8) is similar to the Pacific showing a vertically stratified structure. Again, the equatorial domes are not produced by a purely buoyancy driven model. Strong vertical mixing is visible in the North Atlantic where deep water is formed. This is in general agreement with the data. The deep ocean does not show the cooler ACC waters reaching the ocean bottom.

Fig. 9 gives the model (a) and Levitus (b) salinity fields of the Atlantic. The model again reproduces the inverse stratification at low latitudes. A prominent observed feature of the Atlantic is the intrusion of fresh thermocline water from the ACC, beneath which saltier water penetrates from the north to form a *salt wedge* in the deep ocean. Both structures are present in the model although the intrusion of Antarctic intermediate water proceeds too far north in the model.

In spite of the various idealizations both temperature and salinity fields of the Atlantic and Pacific are reproduced fairly realistically. In particular, the model is able to show accurate salinity structures for both Pacific and Atlantic. These are very different in the two ocean basins. In the Pacific the low latitude intermediate water shows a well mixed region which is enclosed by fresh water tongues in the North and the South Pacific.

The corresponding Atlantic water, on the other hand, is dominated by a fresh water wedge emanating from the ACC and overlying a salt water wedge from the north. Both phenomena are present in the model fields, which suggests that the observed T and S structure in the two ocean basins are direct evidence for the presence of interocean thermohaline flow. The most important differences between the model and observed fields are within the ACC, the meridional structure of which the model makes no attempt to resolve.

In summary, the present 2-dimensional ocean model reproduces the global thermohaline circulation proposed by Gordon (1986) and is capable of modelling the main structure of the latitude-depth distribution of both temperature and salinity. The importance of atmospheric water vapour transport for the maintainance of this interocean exchange of water is demonstrated.

5. Stability of the Pacific-Atlantic interocean circulation

It has often been argued in recent years that the ocean circulation might have more than one stable mode of operation. Transitions between different equilibria can be triggered by fresh water flux anomalies; these occur naturally during the termination of ice ages. The most recent termination, the transition into the present Holocene which started about 14,000 years ago, caused the complete melting of the Laurentian and several other, smaller ice sheets in the northern hemisphere. Denton & Hughes (1981) estimate that $30 \cdot 10^6$ km^3 melted during a period of about 8000 years. Assuming the simplest possible scenario, i.e. that this volume was released at a constant rate of about 0.12 Sv into a 6.5° latitude belt over the Atlantic (corresponding to the resolution of grid B), we get a flux anomaly of about 0.78 myr^{-1}. Broecker *et al.* (1985) suggested, that the river discharge changed from the Mississippi, at the earlier stages of the melting, to the St.

Lawrence later. Several other melting scenarios have been proposed, and Fairbanks (1989) reported a recent reconstruction. These scenarios will be tested elsewhere.

Two experiments are conducted on grid B with $K_v = 0.4 \cdot 10^{-4}$ $m^2 s^{-1}$. The model is spun-up from rest under the restoring boundary conditions (1a) and (2). At t = 7000 yr mixed conditions are applied at which time the natural variability discussed above sets in. The perturbation experiments start at t = 8000 yr from the circulation given in Fig. 3c. A salt flux anomaly corresponding to a fresh water flux of 0.78 myr^{-1} (Exp. I) is applied at 15°N for 4000 yr and then moved to 45°N for another 4000 yr to model the change in discharge location. At t=16,000 yr the anomaly is shut off, and the system was integrated until t = 17,000 yr. Experiment II tests the same scenario for half the anomaly, i.e. 0.39 myr^{-1}.

Fig. 10 displays the meridional overturning at t = 12,000 yr for Exp. I (a) and II (b). The realistic anomaly of Exp. I causes a break-down of the global conveyor belt and a *complete reversal* of the North Atlantic thermohaline circulation. Deep water is now formed in the South Atlantic, and the North Atlantic shows upwelling. The flow in the Pacific, on the other hand, has not changed much, except that sinking in the ACC region now reaches deeper depths. Interocean exchange has stopped, and the two basins exhibit rather independent fields. This state changes little over the next 4000 yr while the flux anomaly continues at the higher latitude. Once the flux anomaly is shut off, the North Pacific cell decreases in strength, but the final steady state obtained at t = 27,000 yr (10,000 yr after the anomaly was switched off) has still one cell in each basin with downwelling in the ACC region. When only half the anomaly is applied (Fig. 10b), the global thermohaline circulation remains in operation, and only the shallow

South Atlantic cell is intensified. After the anomaly is shut off the system returns to the original equilibrium state of Fig. 3c.

These two experiments demonstrate that the model possesses two stable states of the coupled Pacific-Atlantic basin system under the same forcing. A realistic flux anomaly is capable of causing a transition from the state with interocean exchange to a state, in which the thermohaline circulation of Pacific and Atlantic operate independently. The oceanic heat transport is dramatically different for the two states. Fig. 11 compares the meridional heat transport of the spin-up (solid),and Exp. I (dashed) and Exp. II (dash-dotted) at t=12,000 yr. In Exp. I the Atlantic heat flux is to the south with very little transport in the highest latitudes. In the Pacific, on the other hand, modifications are only minor. Exp. II shows changes only in the South Atlantic, where the heat flux is increased. Again, the Pacific flux is unaltered.

It is the vertical ocean-atmosphere heat flux from which we expect climatic changes that would be detected in proxy data. Tab. 3 shows the average vertical heat flux in the North Atlantic from 50°N to 80°N (a), and in the North Pacific from 41°N to 50°N (b). Changes in the North Pacific are too small to cause a detectable signal in any proxy record. However, in the Atlantic the heat flux reduces by 25 Wm^{-2} for Exp I. and 3.3 Wm^{-2} in Exp. II. These correspond, using the grey body radiation estimate, to an atmospheric temperature change of order -9°C and -1.2°C, respectively. Both signals could, if present, be found in oxygen isotope records. The picture here is consistent with Broecker *et al.* (1985) who find the Younger Dryas signal only in locations which are under the influence of the North Atlantic (Europe, Greenland and the Canadian maritime) but not where the North Pacific determines the climate (central and west North America).

6. Conclusions

The model developed in Part I was extended to simulate a possible global thermohaline circulation which connects the Pacific and Atlantic and allows for interocean exchange of mass and heat. The state obtained under restoring boundary conditions with an identical salinity distribution for both basins consists of a 2-cell circulation in both Pacific and Atlantic. Atlantic deep water formation is more pronounced due to the increased northward extent of this basin. The main area of deep water production, however, is the ACC region. Upon a switch to mixed boundary conditions the system shows a transition with strong interocean exchange of water. The final steady state is one with deep water formation in both high northern latitudes and very little cross basin flow.

A global thermohaline circulation proposed by Gordon (1986) could be realized by restoring to an asymmetric surface salinity profile that is fresher in the Pacific; this corresponds to present-day conditions. Deep water is now formed only in the North Atlantic from where it spreads into the Pacific to upwell. The state is stable under mixed boundary conditions. We have also shown that the present geographical extension of Pacific and Atlantic basin favours a conveyor belt circulation of this nature.

The global circulation is maintained by a net fresh water flux from the Atlantic to the Pacific through the atmosphere. If this flux is removed, the oceanic circulation changes on a comparatively short time scale (here 1500 yr) to a state, in which deep water is formed at both northern latitudes with no interocean exchange. This emphasizes the key importance of the hydrological cycle in determining the thermohaline flow and hence the direction of the oceanic heat flux.

Depending on the value of the vertical diffusivity natural variability of the flow could be observed in the form of a self-sustained oscillation. Meridional heat flux, as well as latitude-depth structure of temperature and salinity agree well with observed data.

We analyzed the stability of this interocean flow by conducting a realistic deglaciation experiment. The stable state under mixed boundary conditions was perturbed by a salt flux (negative fresh water flux) anomaly of 0.1 Sv and 0.05 Sv during 8000 years. The strong anomaly causes the Atlantic circulation to reverse completely thereby inhibiting any cross basin flow. Eventually, the stable 1-cell circulation is reached in each basin individually. The global flow persisted, however, for the weaker anomaly and exhibited decreased ocean-atmosphere heat fluxes in the North Atlantic. For both scenarios the Pacific thermohaline circulation did not change much; this is consistent with the spatial distribution of the Younger Dryas climate event (Broecker *et al.*, 1985).

The deglaciation experiment showed that the global thermohaline circulation, which results from realistic surface forcing, is stable for small perturbations. However, a second stable state under identical surface forcing exists; in this state there is no interocean exchange, and the thermohaline circulations of Pacific and Atlantic basin operate independently. A transition is possible for salt flux anomalies exceeding a threshold value which is within present estimates of glacial melt water fluxes at the last termination.

The present paper emphasizes the significance of the thermohaline circulation of the ocean for internal fluctuations of the climate system and climate change. It is shown that both natural variability (on time scales of decades and longer) and multiple equilibria are realized under present day

forcing. The atmospheric hydrological cycle plays a crucial role as a motor of the thermohaline circulation. The eventual goal is to combine the present model with 2-dimensional models of the atmosphere and the cryosphere in order to obtain a realistic and yet inexpensive model suitable for paleoclimatic studies.

Acknowledgements:

Fellowship 82.613.0.88 of the Swiss National Science Foundation awarded to TFS is acknowledged. This work was also partly supported by research grants from the Canadian Natural Sciences and Engineering Research Council and Atmospheric Environment Service awarded to L.A. Mysak.

References:

Baumgartner A., E. Reichel, 1975, *The World Water Balance*. Elsevier, 179pp.

Broecker W.S., D.M. Peteet, D. Rind, 1985, Does the ocean-atmosphere system have more than one stable mode of operation? *Nature*, **315**, 21-26.

Bryan F., 1987, Parameter sensitivity of primitive equation ocean general circulation models. *J. Phys. Oceanogr.*, **17**, 970-985.

Cox M.D., 1989, An idealized model of the world ocean. Part I: The global-scale water masses. *J. Phys. Oceanogr.*, **19**, 1730-1752.

Fairbanks R.G., 1989, A 17,000-year glacio-eustatic sea level record: influence of glacial melting rates on the Younger Dryas event and deep-ocean circulation. *Nature*, **342**, 637-642.

Fiadeiro M.E., G. Veronis, 1977, On weighted-mean schemes for the finite-difference approximation to the advection-diffusion equation. *Tellus*, **29**, 512-522.

Gordon A.L., 1986, Interocean exchange of thermocline water. *J. Geophys. Res.*, **91**, 5037-5046.

Levitus S., 1982, Climatological atlas of the world ocean. *NOAA Prof. Paper*, **13**, 173pp.

Maier-Reimer E., U. Mikolajewicz, 1989, Experiments with an OGCM on the cause of the Younger Dryas. In *Oceanography*, A. Ayala-Castañares, W. Wooster and A. Yáñez-Arancibia (eds.), UNAM Press, 87-100.

Marotzke J., P. Welander, J. Willebrand, 1988, Instability and multiple equilibria in a meridional-plane model of the thermohaline circulation. *Tellus*, **40A**, 162-172.

Stommel H., 1961, Thermohaline convection with two stable regimes of flow. *Tellus*, **13**, 224-230.

Warren B.A., 1981, Deep circulation of the world ocean. In *Evolution of Physical Oceanography, Scientific Surveys in Honor of Henry Stommel*, B.A. Warren and C. Wunsch (eds.)., MIT Press, 6-41.

Weaver A.J., E.S. Sarachik, 1990, Evidence for decadal variability in an ocean general circulation model: an advective mechanism. *Atmosphere-Ocean*, (submitted).

Wells N.C., C. Mead, 1989, ocean models and the inter-basin transport of heat. In *Ocean circulation models: combining data and dynamics*, D.L.T. Anderson and J. Willebrand (eds.), Kluwer, (preprint).

Wright D.G., T.F. Stocker, 1990, A zonally averaged model for the thermohaline circulation. Part I: Model development and flow dynamics. *J. Phys. Oceanogr.* (submitted).

Tables:

	Heatflux [10^{-3} Wm^{-2}]	Saltflux [10^{-2} $ppt \cdot m^{-2}s^{-1}$]
1 kyr	-12	-1.0
2 kyr	-14	-0.33
4 kyr	-1.8	-0.032
6 kyr	-0.63	-0.0058
7 kyr	-0.12	-0.0027

Table 1: Convergence of the basin average vertical heat and salt flux during spin-up under restoring boundary conditions (54a) and (64) on grid A.

grid	K_V [$10^{-4}m^2s^{-1}$]	τ_H [days]	North Atlantic Overturning [Sv]	max. meridional heat flux [PW] Atlantic (north)	Pacific (south)
A	0.4	100	16.9	0.81	0.63
B	0.4	100	17.0	0.74	0.60
B	0.8	100	20.2	0.92	0.78
C	0.4	100	11.9	0.41	0.40
C	0.8	50	17.2	0.59	0.62

Table 2: Comparison of maximum transport and meridional heat flux for different grid resolutions (A=15×10, B=31×10, C=31×20), vertical diffusivities and relaxation time scales.

Salt flux anomaly		t= 8000 yr	12,000	16,000	17,000
Exp.I	0.78 myr^{-1}	12.4 Wm^{-2}	-12.6	-12.6	-12.7
Exp.II	0.39	12.4	9.9	8.7	11.4

Table 3a: Average vertical heat flux in the North Atlantic between 50°N and 80°N:

Salt flux anomaly		t= 8000 yr	12,000	16,000	17,000
Exp.I	0.78 myr^{-1}	8.29 Wm^{-2}	7.85	7.84	7.59
Exp.II	0.39	8.29	8.27	8.39	8.29

Table 3b: Average vertical heat flux in the North Pacific between 41°N and 50°N:

Figure Captions:

Figure 1: Contours of the meridional overturning streamfunction in Sv (1 Sv = $10^6 m^3 s^{-1}$) in the Pacific-Atlantic basin system. The Pacific extends from 50°N (left) to 55°S, where it joins the Atlantic basin extending to 80°N (right). The Antarctic Circumpolar Current region (ACC) is located within the two vertically dashed lines. The steady state under symmetric temperature and salinity restoring boundary condition (a) is unstable upon a switch to mixed boundary conditions and undergoes a transition (b) to the final steady state (c).

Figure 2a: Latitude profile of the restoring temperature in °C (solid), Levitus (1982) zonal average (dashed) and vertical surface heat flux in Wm^{-2} (dash-dotted) of the steady state of Fig. 3b.

Figure 2b: Latitude profile of the restoring salinity in ppt (solid), Levitus (1982) zonal average (dashed) and vertical salt flux expressed as an equivalent fresh water flux P-E in m/yr (dash-dotted) of the steady state of Fig. 3b.

Figure 3a: Under restoring boundary conditions using realistic sea surface salinity (Fig. 2b, solid), a global thermohaline circulation results. The steady state on grid A, evolving from 7000 yr of spin-up, shows deep water forming only in the North Atlantic, part of which is returned to form intermediate South Atlantic water. The rest spreads into the Pacific, where it upwells. Thermocline flow is to the south in the Pacific and to the north in the Atlantic. Surface forcing and fluxes are shown in Fig 2.

Figure 3b: Further integration on grid A over 5000 yr under mixed boundary conditions shows a state almost identical to Fig. 3a; the global thermohaline circulation is stable.

Figure 3c: Same as Fig. 3b for double horizontal resolution (grid B).

Figure 3d: Same as Fig. 3b for double horizontal and vertical resolution (grid C).

Figure 4: Time series of the maximum (solid) and minimum (dashed) streamfunction of the state in Fig. 3b under mixed boundary conditions. Natural variability in the form of a self-sustained oscillation with a period of 38 years is observed. Vertical diffusivity here is $K_v = 0.4 \cdot 10^{-4} m^2 s^{-1}$; the variability disappears for larger veritcal diffusivity and higher vertical resolution.

Figure 5a: Meridional overturning streamfunction of the steady state at t = 8000 yr under mixed boundary conditions on grid C with $K_v = 0.8 \cdot 10^{-4}$ $m^2 s^{-1}$ and τ_H = 50 dy.

Figure 5b: Sea surface temperature (solid), Levitus (1982) zonal averages (dashed) and vertical heat flux (dash-dotted) of the steady state in Fig. 5a.

Figure 5c: Sea surface salintity (solid), Levitus (1982) zonal averages (dashed) and vertical salt flux (dash-dotted) of the steady state in Fig. 5a.

Figure 5d: Meridional heat transport in PW (1 PW = 10^{15} W) integrated over the respective basin for the state in Fig. 5a. Heat is transported mainly to the south in the Pacific and to the north in the Atlantic.

Figure 6: Comparison of the zonally averaged temperature field in the Pacific for the steady state in Fig. 5a, (a), with the observed temperature from Levitus (1982), (b).

Figure 7: Comparison of the zonally averaged salinity field in the Pacific for the steady state of Fig. 5a, (a), with Levitus (1982), (b).

Figure 8: Comparison of the zonally averaged temperature field in the Atlantic for the steady state in Fig. 5a, (a), with Levitus (1982), (b).

Figure 9: Comparison of the zonally averaged salinity field in the Atlantic for the steady state of Fig. 5a, (a), with Levitus (1982), (b).

Figure 10: The steady state global thermohaline circulation under mixed boundary conditions of Fig. 3c is perturbed by an Atlantic fresh water flux anomaly of 0.78 myr^{-1} for (a) and 0.39 myr^{-1} for (b), applied at 15°N for 4000 yr and then at 50°N for 4000 yr. The strong anomaly causes the Atlantic circulation to reverse (a), while the weak anomaly intensifies only the shallow South Atlantic cell (b).

Figure 11: Meridional heat transport in PW integrated zonally over the respective basin for the states in Fig. 3c (solid), 10a (dashed) and 10b (dash-dotted).

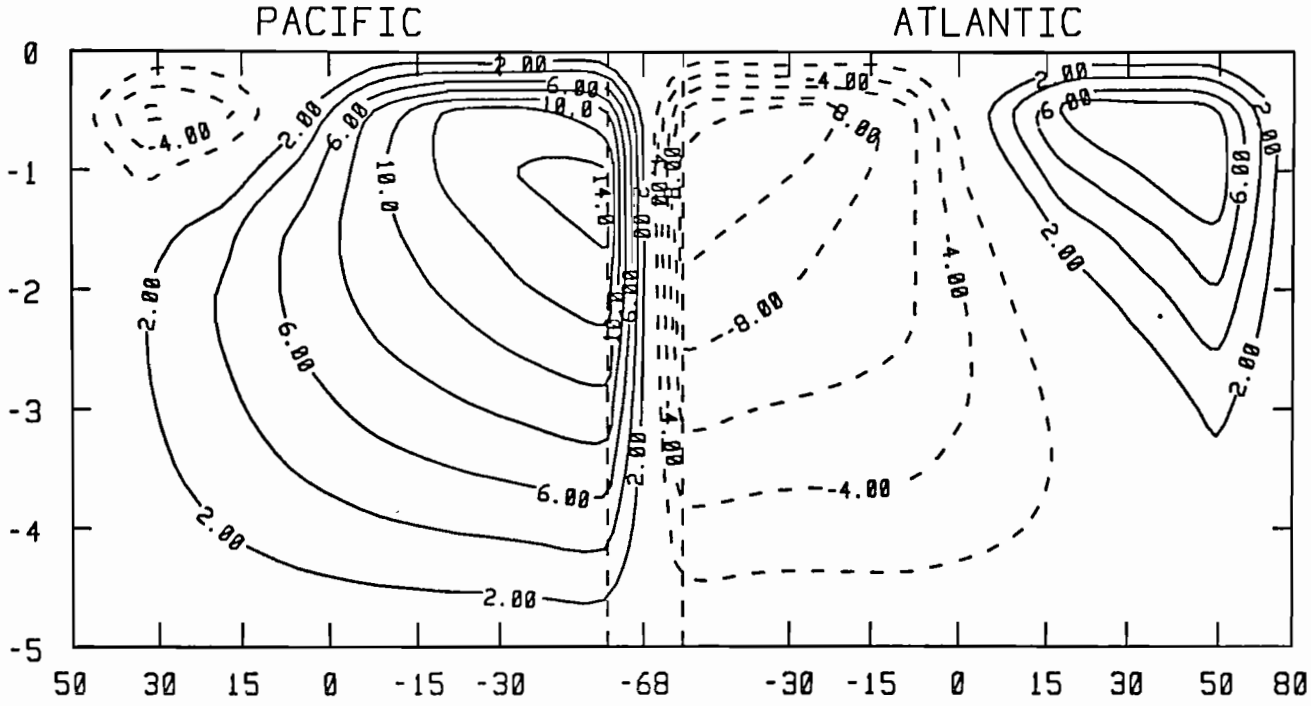
PACIFIC
ATLANTIC
0
-1
-2
-3
-4
-5
50
30
15
0
-15
-30
-68
-30
-15
0
15
30
50
80

Fig 1a:

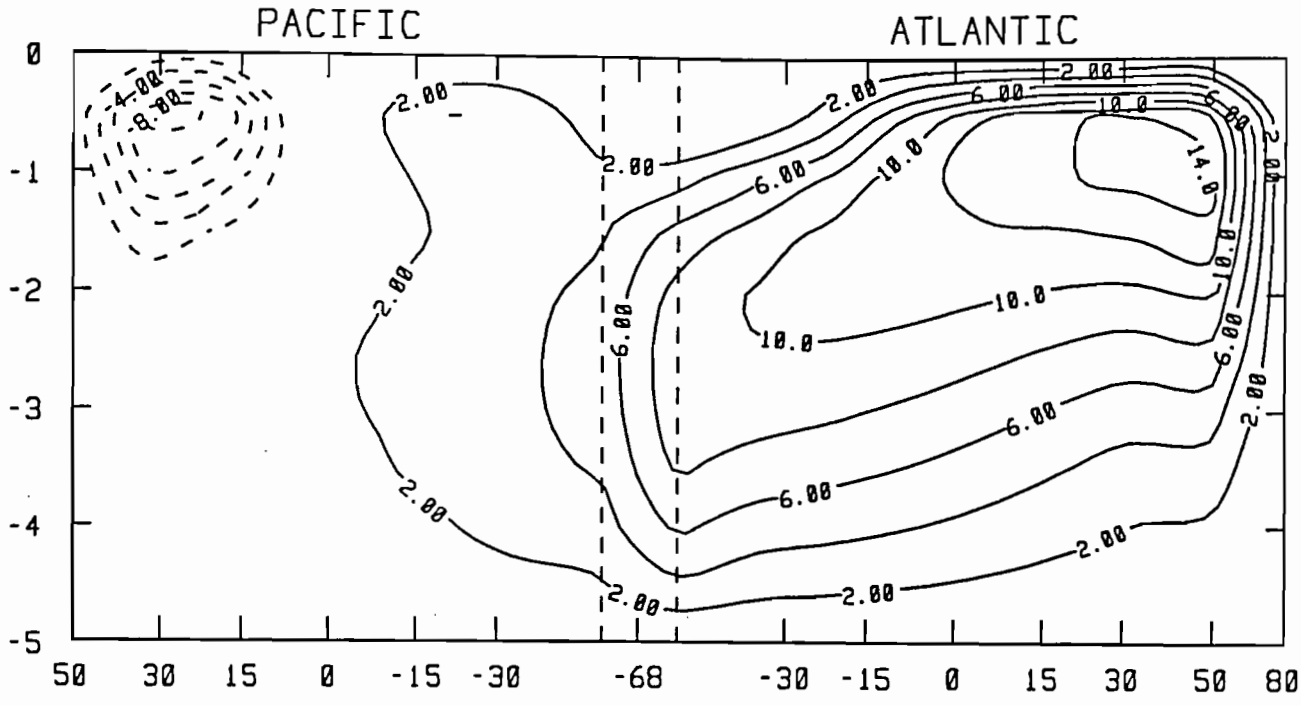
PACIFIC
ATLANTIC
0
-1
-2
-3
-4
-5
50
30
15
0
-15
-30
-68
-30
-15
0
15
30
50
80

Fig 1b

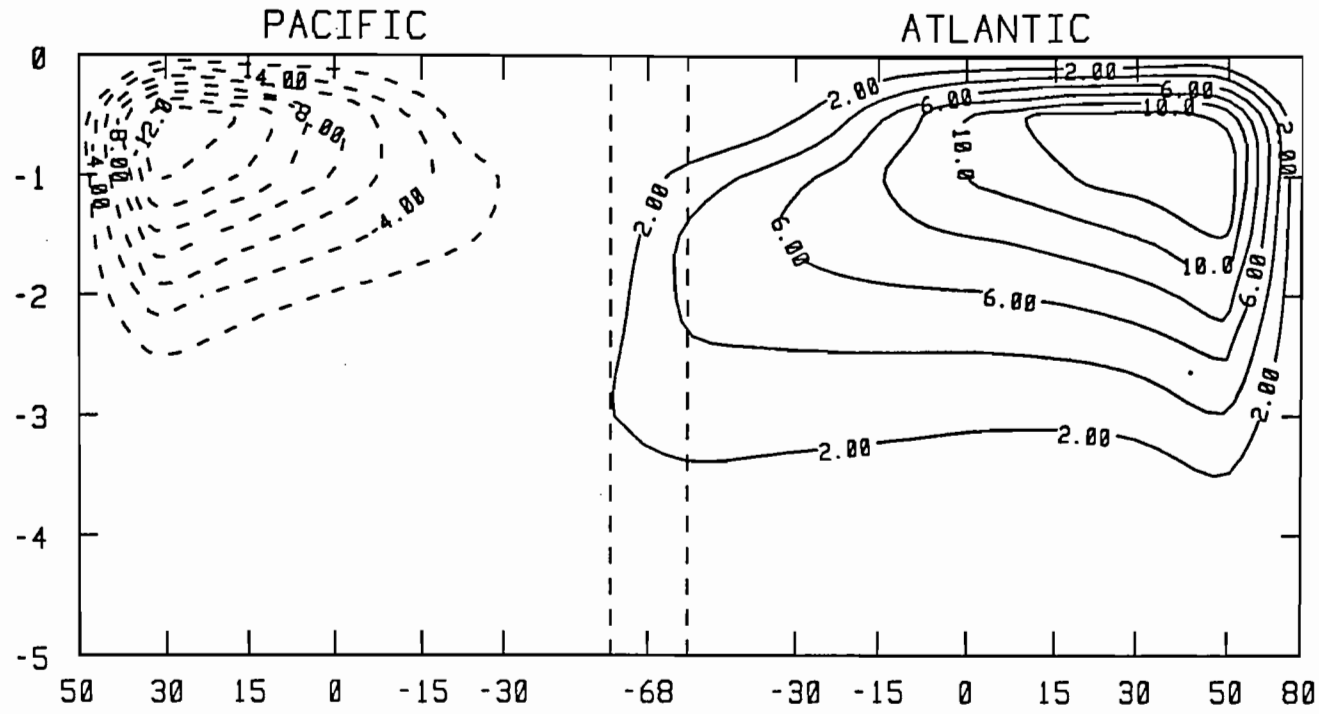
PACIFIC
ATLANTIC
0
-1
-2
-3
-4
-5
50
30
15
0
-15
-30
-68
-30
-15
0
15
30
50
80
-12.00
-8.00
-4.00
2.00
6.00
10.0

Fig 1c

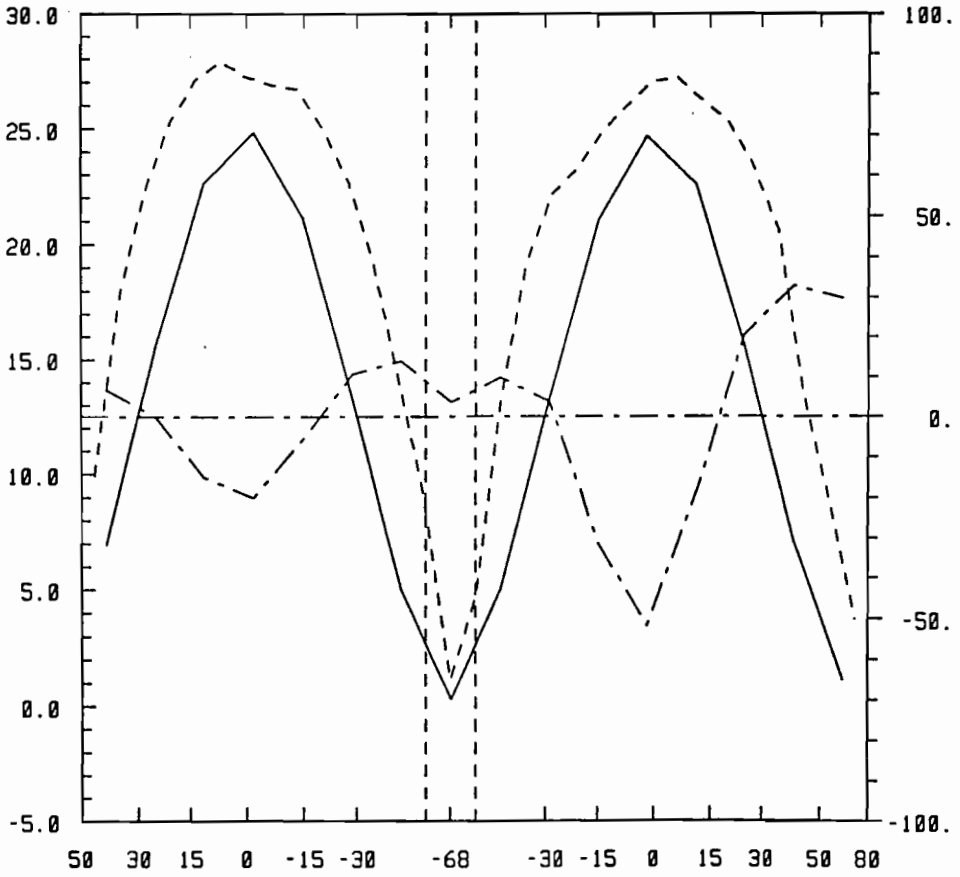
30.0
25.0
20.0
15.0
10.0
5.0
0.0
-5.0
100.
50.
0.
-50.
-100.
50 30 15 0 -15 -30 -68 -30 -15 0 15 30 50 80

Fig 2a

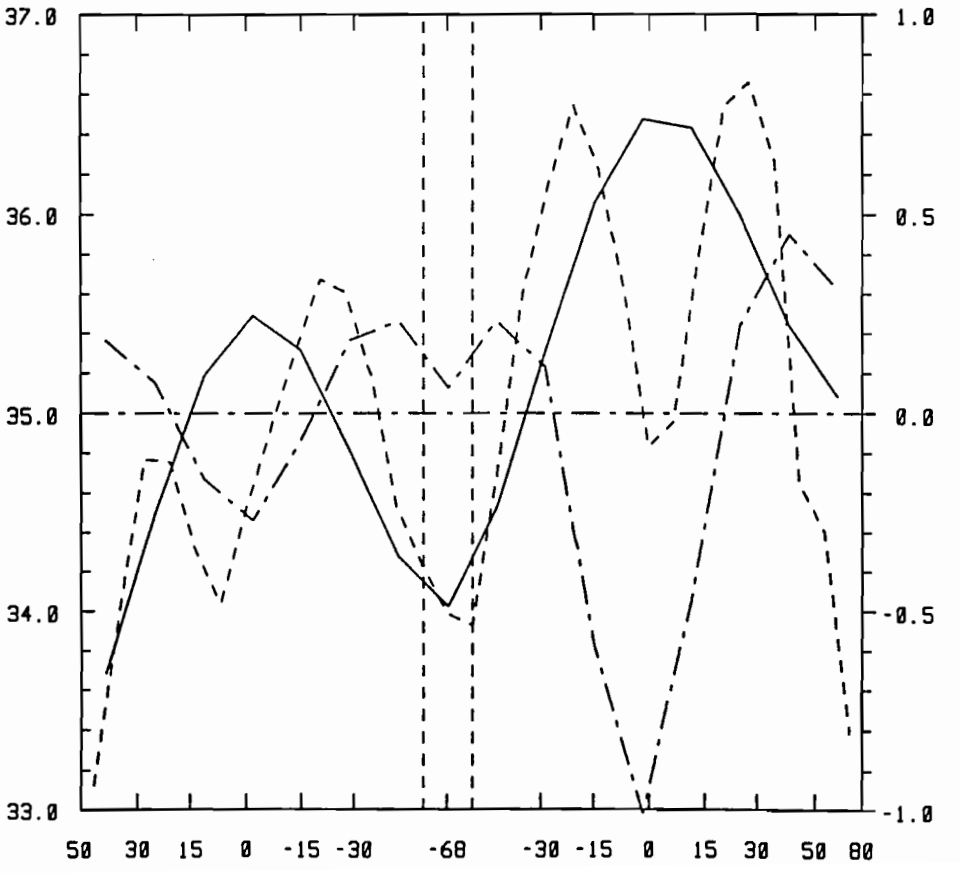
37.0
36.0
35.0
34.0
33.0
1.0
0.5
0.0
-0.5
-1.0
50 30 15 0 -15 -30 -68 -30 -15 0 15 30 50 80

Fig 2b

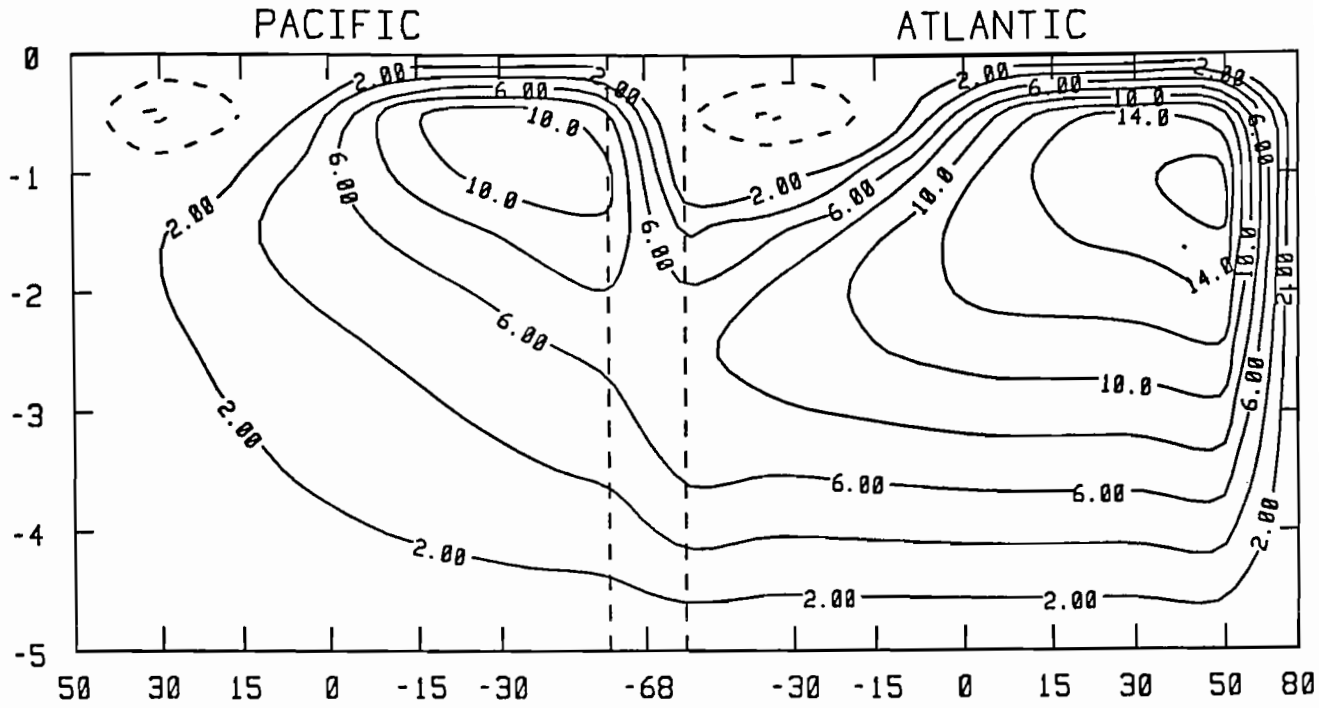
PACIFIC
ATLANTIC
0
-1
-2
-3
-4
-5
50 30 15 0 -15 -30 -68 -30 -15 0 15 30 50 80
2.00
6.00
10.0
14.0

Fig 3a

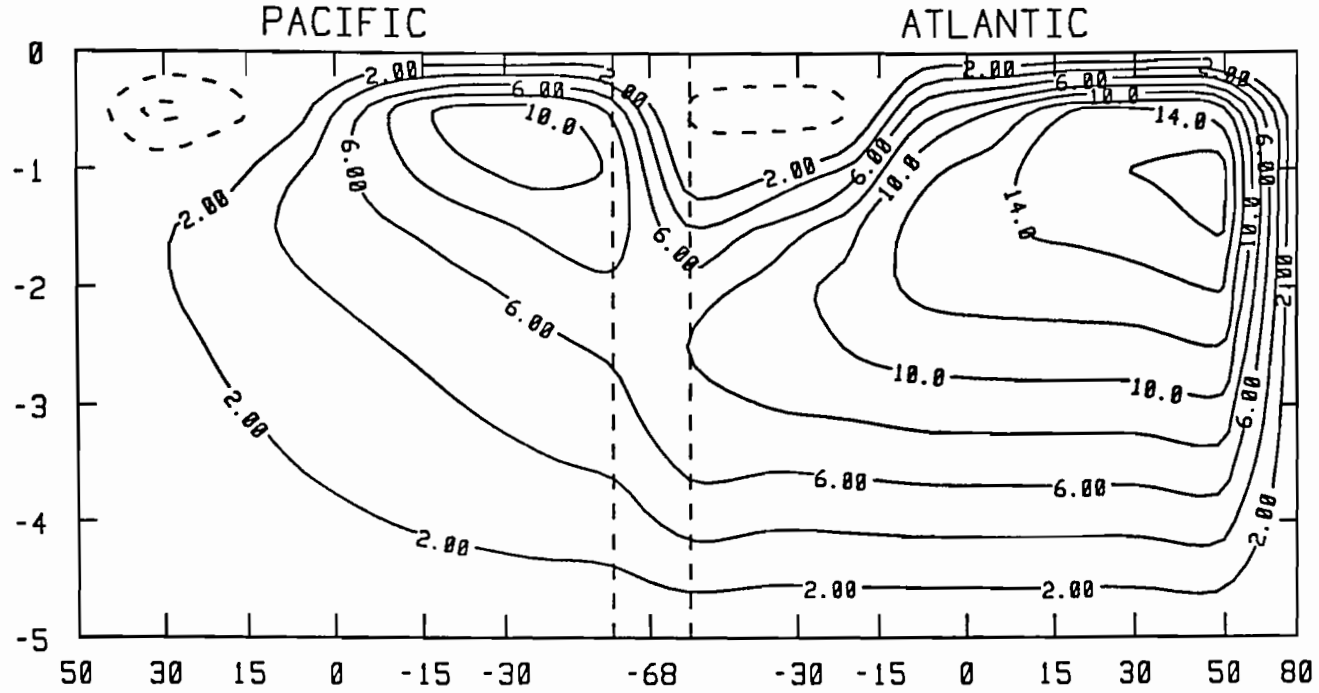
PACIFIC
ATLANTIC
0
-1
-2
-3
-4
-5
50 30 15 0 -15 -30 -68 -30 -15 0 15 30 50 80
2.00
6.00
10.0
14.0

Fig 3b

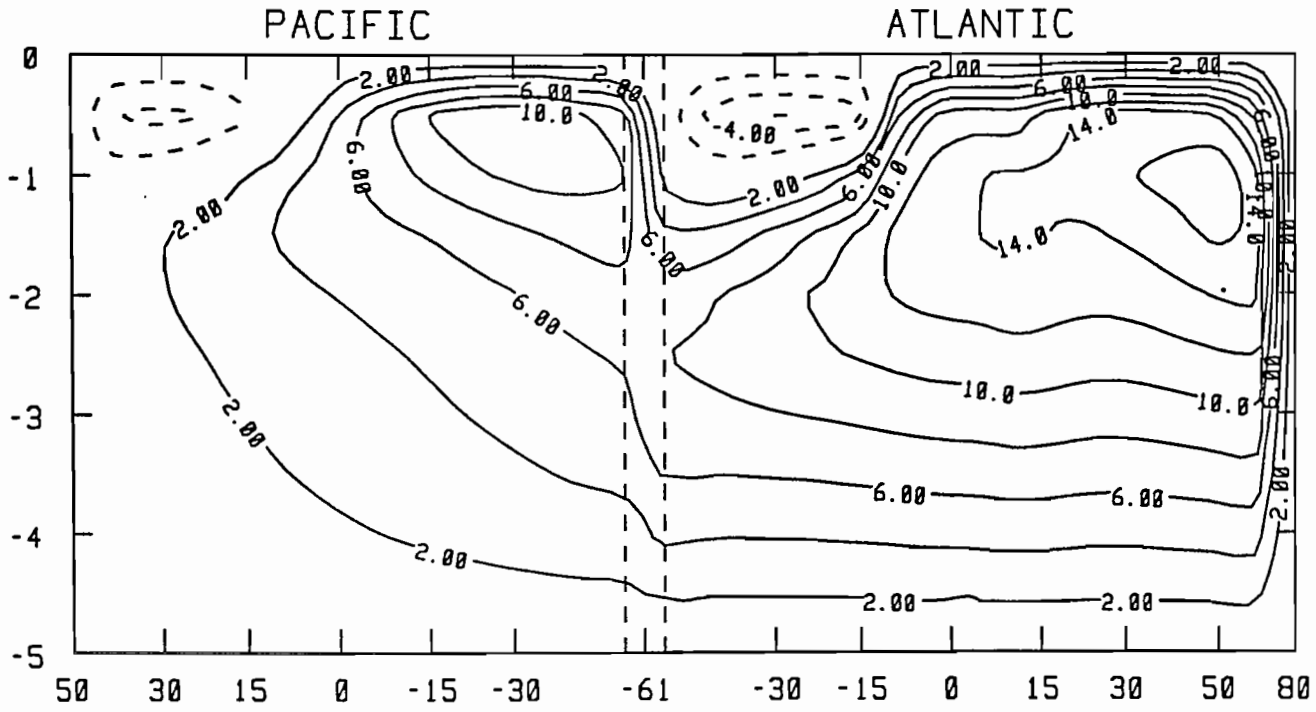
PACIFIC
ATLANTIC
0
-1
-2
-3
-4
-5
50
30
15
0
-15
-30
-61
-30
-15
0
15
30
50
80
2.00
6.00
10.0
14.0
-4.00

Fig 3c

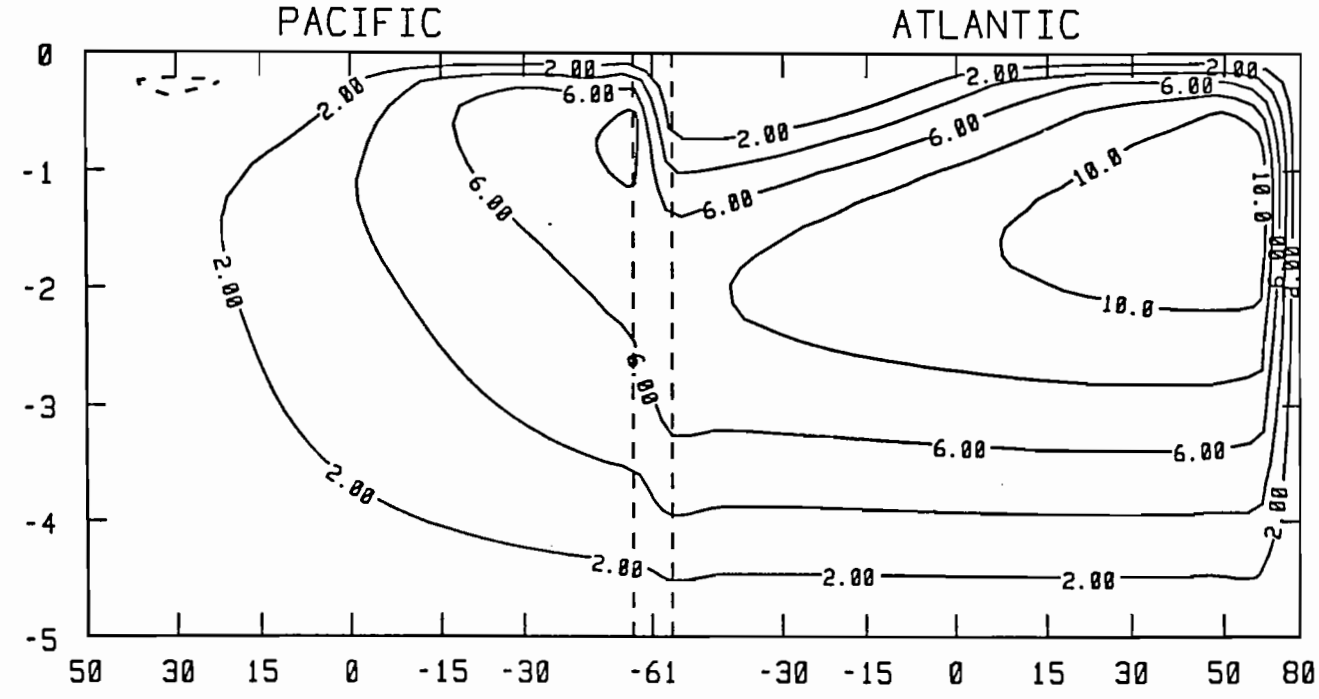
PACIFIC
ATLANTIC
0
-1
-2
-3
-4
-5
50
30
15
0
-15
-30
-61
-30
-15
0
15
30
50
80
2.00
6.00
10.0

Fig 3d

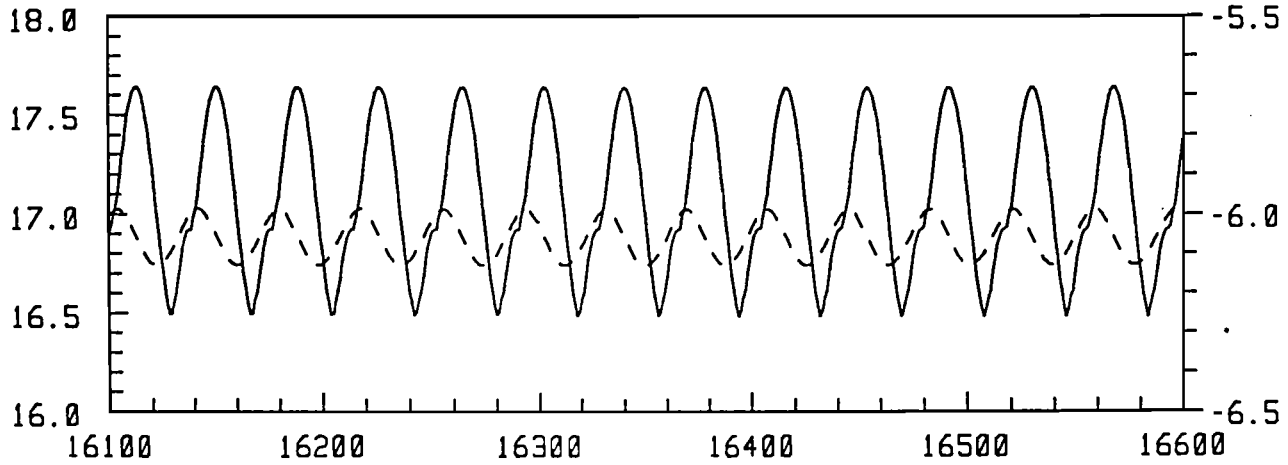
18.0
17.5
17.0
16.5
16.0
-5.5
-6.0
-6.5
16100
16200
16300
16400
16500
16600

Fig 4

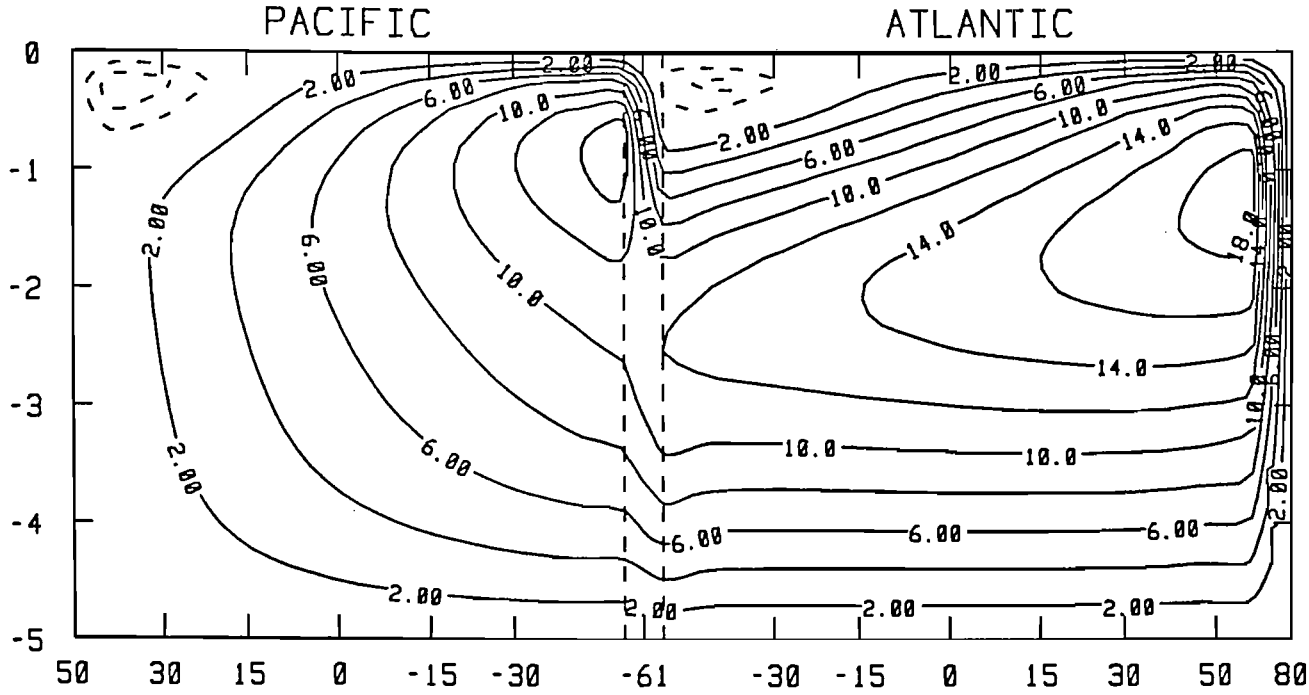
PACIFIC
ATLANTIC
0
-1
-2
-3
-4
-5
50
30
15
0
-15
-30
-61
-30
-15
0
15
30
50
80
2.00
6.00
10.0
14.0

Fig 5a

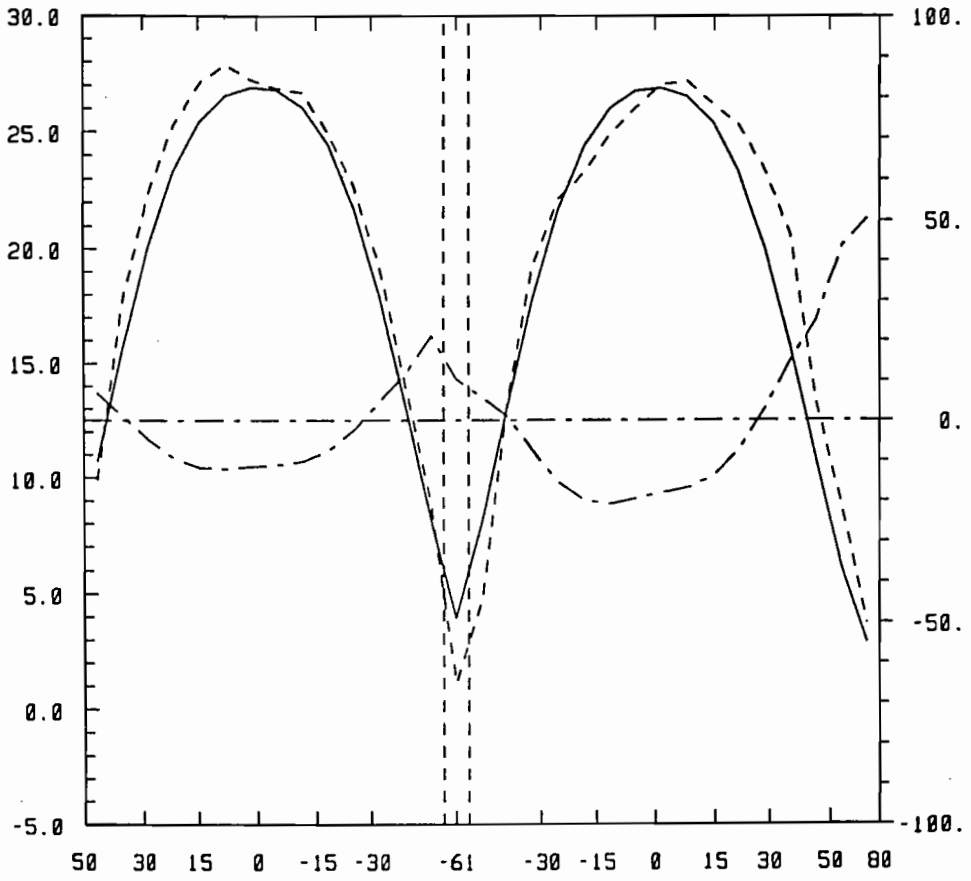
30.0
25.0
20.0
15.0
10.0
5.0
0.0
-5.0
100.
50.
0.
-50.
-100.
50 30 15 0 -15 -30 -61 -30 -15 0 15 30 50 80

Fig 5b

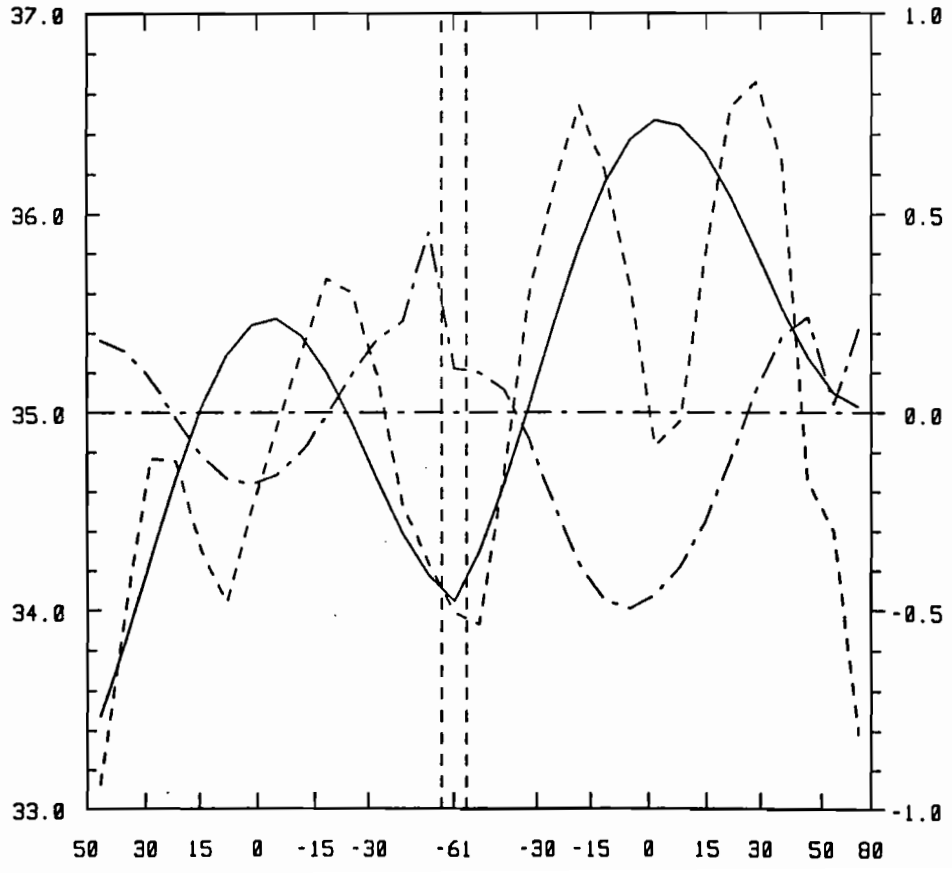
37.0
36.0
35.0
34.0
33.0
1.0
0.5
0.0
-0.5
-1.0
50 30 15 0 -15 -30 -61 -30 -15 0 15 30 50 80

Fig 5c

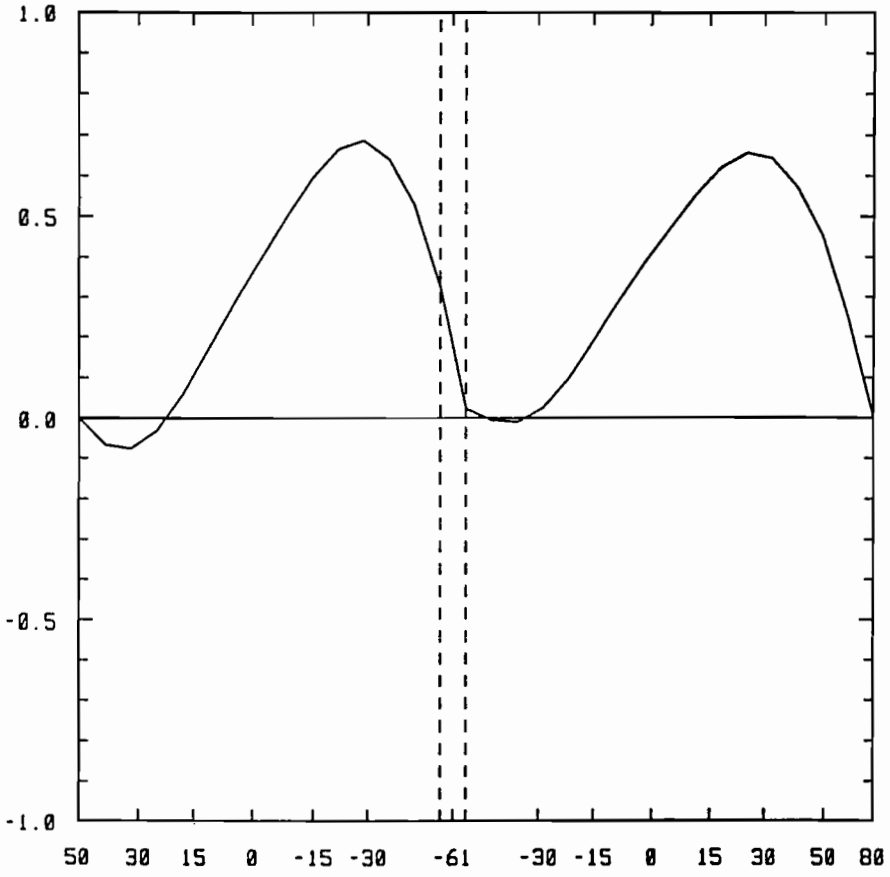

Fig 5d

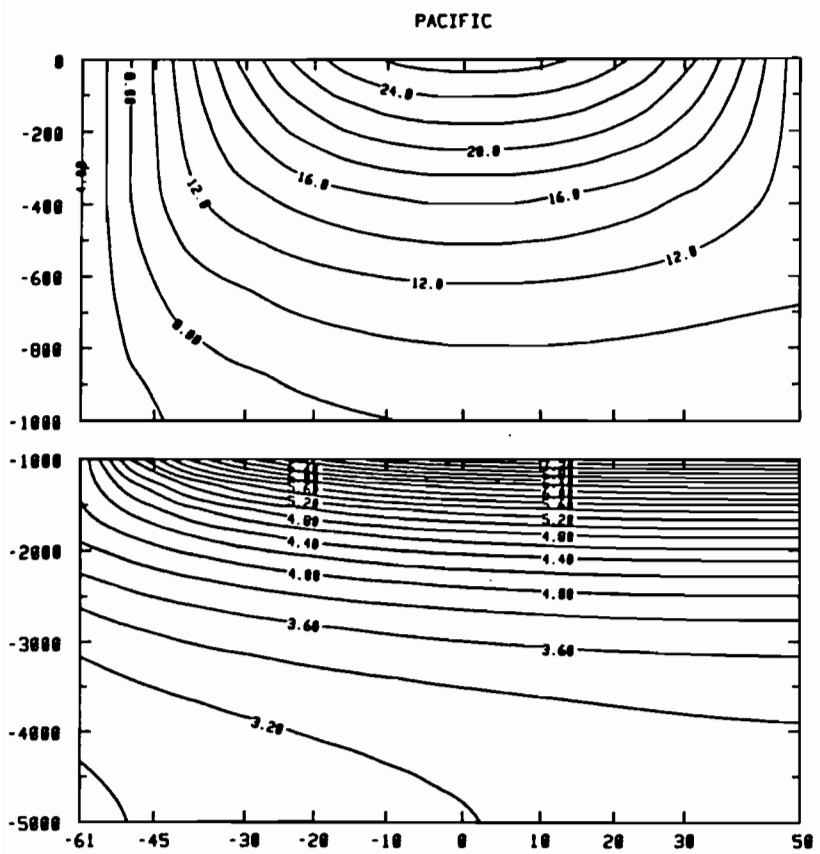
PACIFIC
0
-200
-400
-600
-800
-1000
-1000
-2000
-3000
-4000
-5000
-61
-45
-30
-20
-10
0
10
20
30
50
24.0
20.0
16.0
12.0
8.00
5.20
4.80
4.40
3.60
3.20

Fig 6a

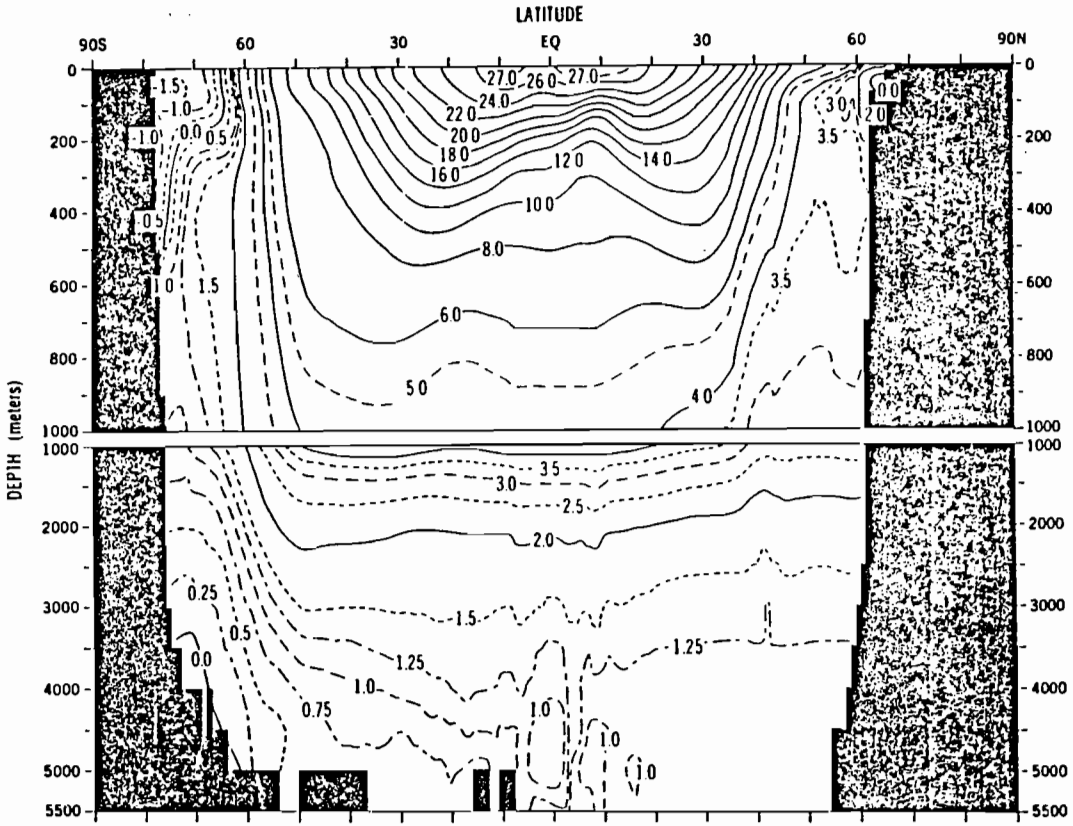
LATITUDE
90S
60
30
EQ
30
60
90N
DEPTH (meters)
0
200
400
600
800
1000
2000
3000
4000
5000
5500
27.0
26.0
24.0
22.0
20.0
18.0
16.0
14.0
12.0
10.0
8.0
6.0
5.0
4.0
3.5
3.0
2.5
2.0
1.5
1.25
1.0
0.75
0.5
0.25
0.0
-0.5
-1.0
-1.5

Fig 6b

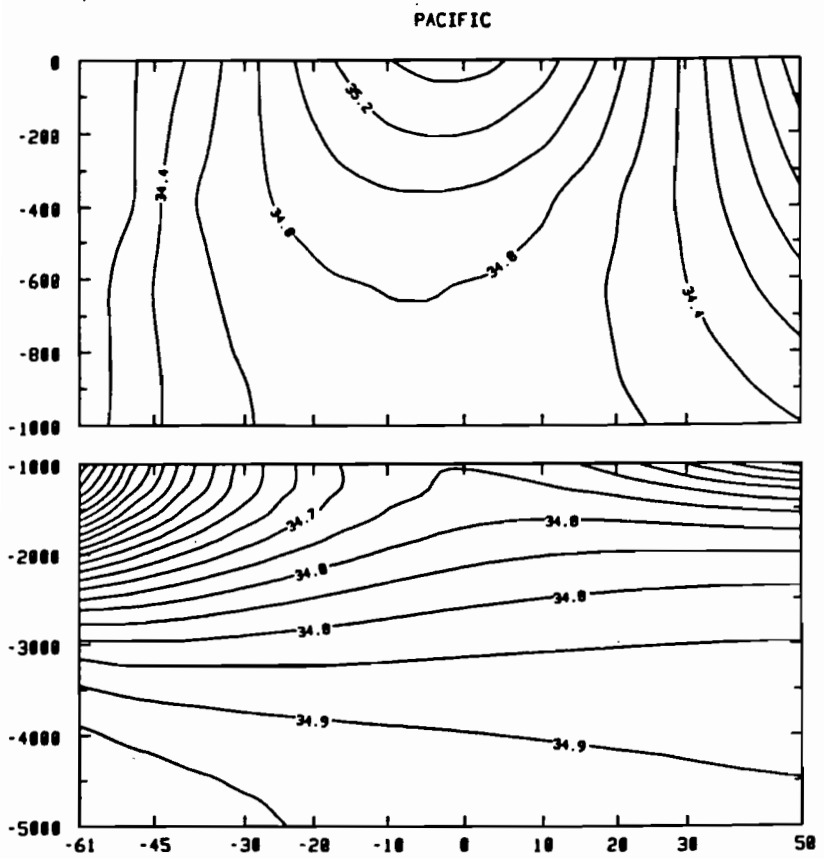
PACIFIC
0
-200
-400
-600
-800
-1000
-1000
-2000
-3000
-4000
-5000
-61
-45
-30
-20
-10
0
10
20
30
50
34.4
35.2
34.6
34.8
34.7
34.9

Fig 7a

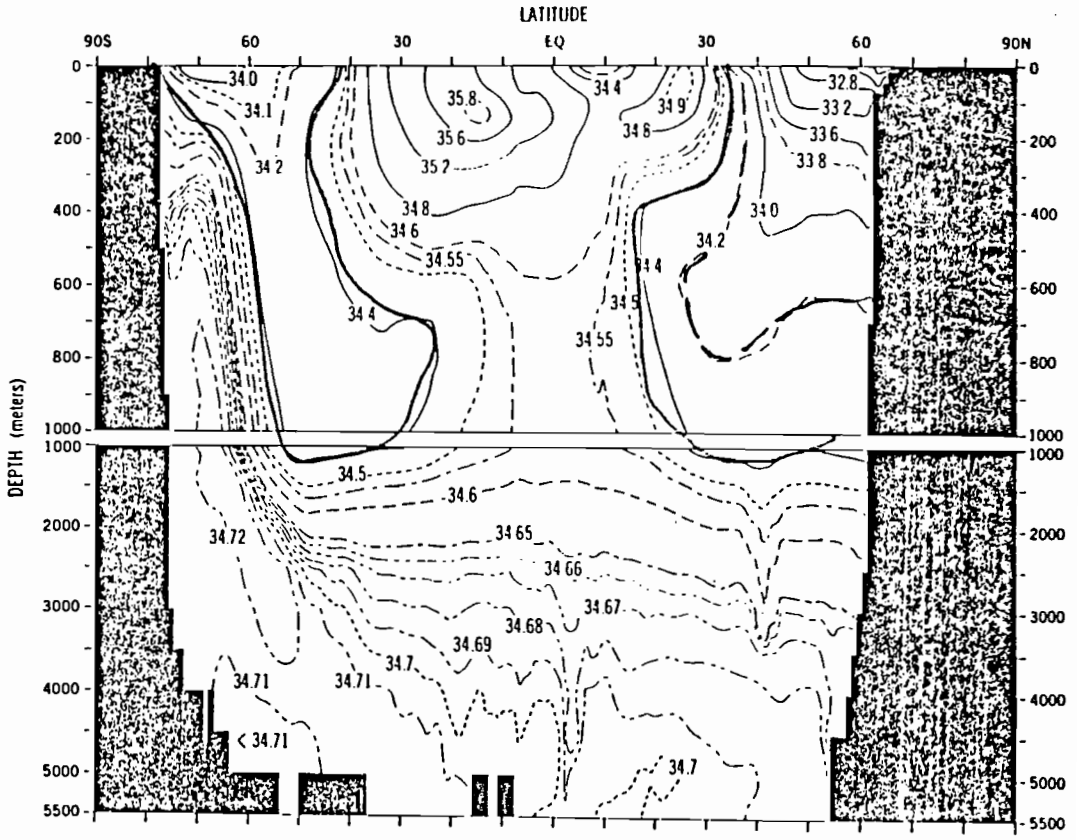
LATITUDE
90S
60
30
EQ
30
60
90N
DEPTH (meters)
0
200
400
600
800
1000
2000
3000
4000
5000
5500
34.0
34.1
34.2
35.8
35.6
35.2
34.8
34.6
34.55
34.4
34.9
34.6
34.4
34.5
34.55
32.8
33.2
33.6
33.8
34.0
34.2
34.5
34.6
34.72
34.65
34.66
34.67
34.68
34.69
34.7
34.71
< 34.71

Fig 7b

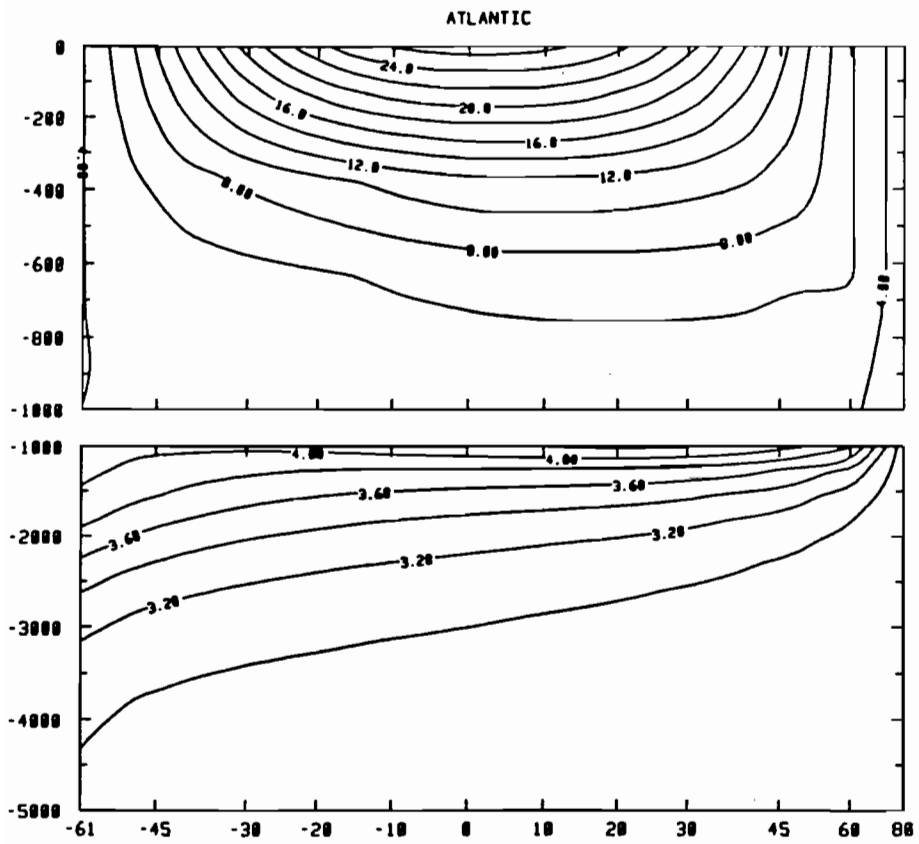
ATLANTIC
0
-200
-400
-600
-800
-1000
-1000
-2000
-3000
-4000
-5000
24.0
20.0
16.0
12.0
8.00
4.00
3.60
3.20
-61
-45
-30
-20
-10
0
10
20
30
45
60
80

Fig 8a

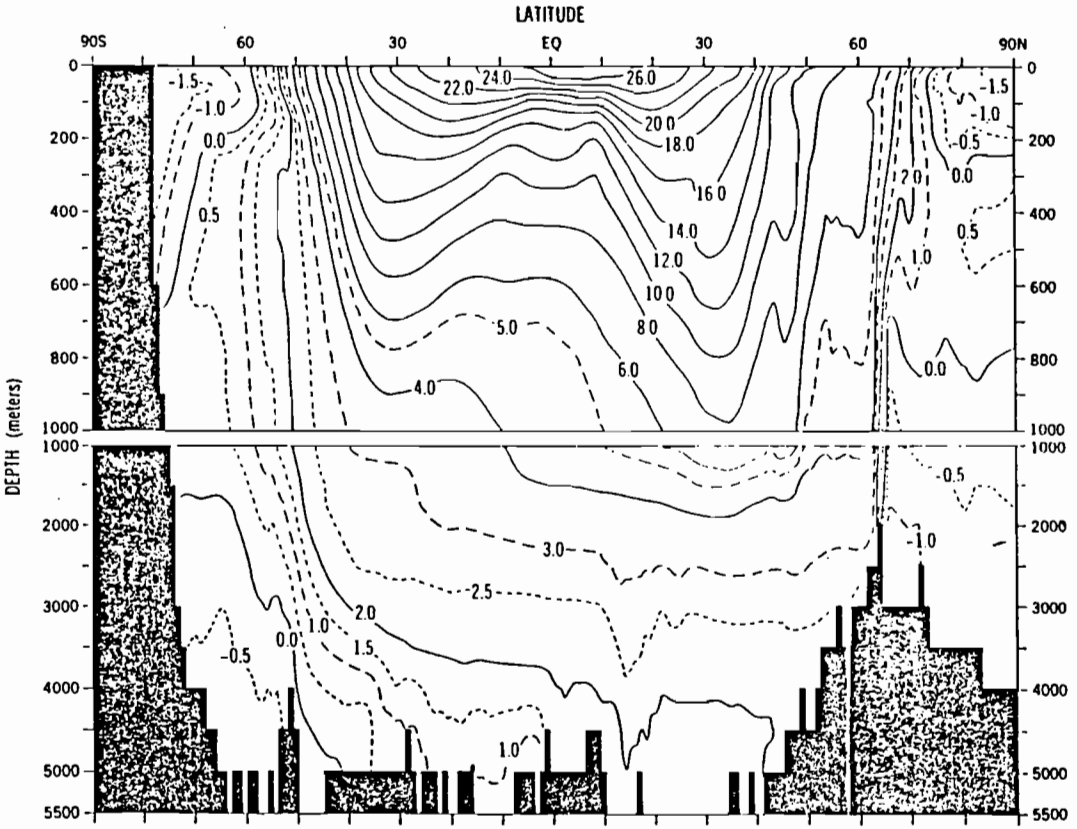
LATITUDE
90S
60
30
EQ
30
60
90N
DEPTH (meters)
0
200
400
600
800
1000
2000
3000
4000
5000
5500
-1.5
-1.0
-0.5
0.0
0.5
1.0
1.5
2.0
3.0
4.0
5.0
6.0
8.0
10.0
12.0
14.0
16.0
18.0
20.0
22.0
24.0
26.0
2.5

Fig 8b

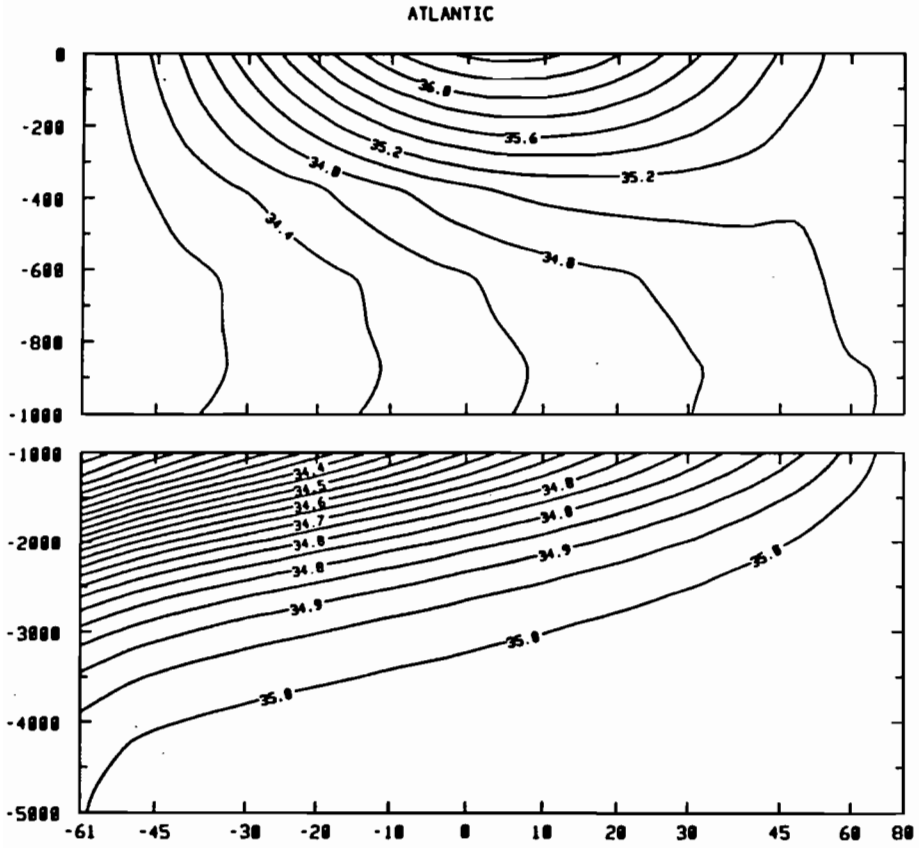
ATLANTIC
0
-200
-400
-600
-800
-1000
-1000
-2000
-3000
-4000
-5000
-61
-45
-30
-20
-10
0
10
20
30
45
60
80
35.8
35.6
35.2
34.8
34.4
34.5
34.6
34.7

Fig 9a

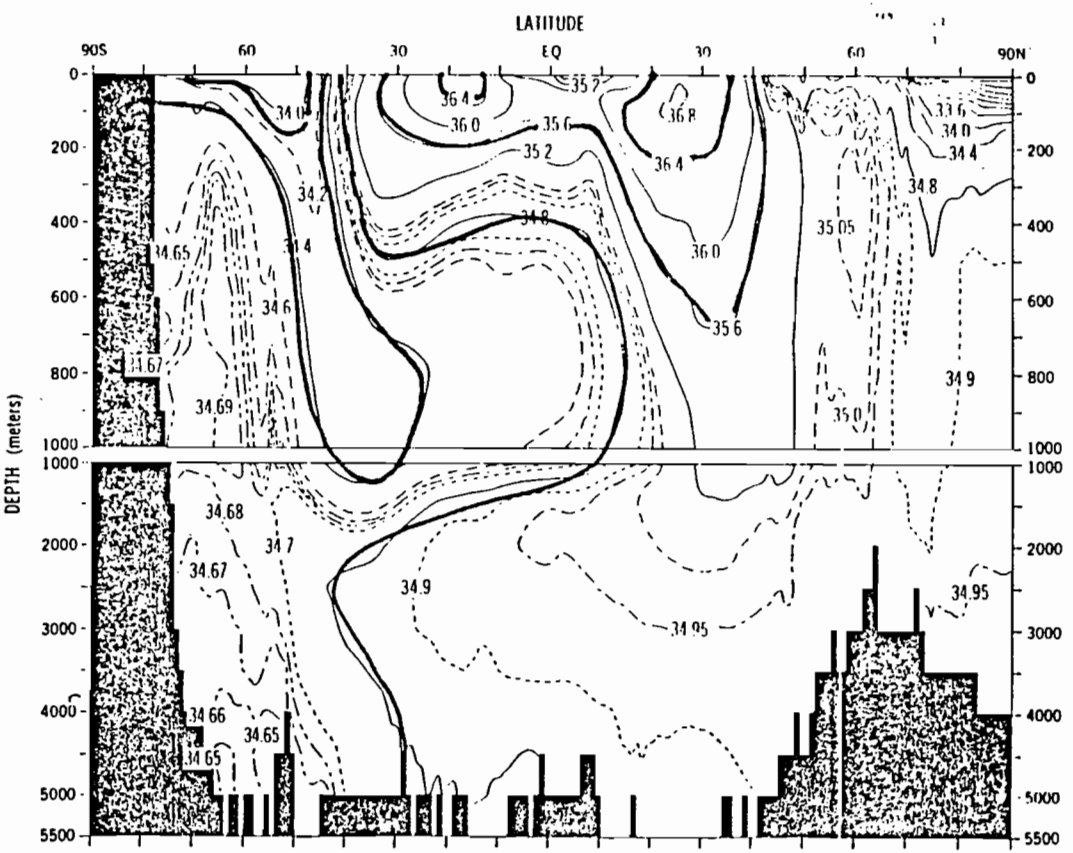
LATITUDE
90S
60
30
EQ
30
60
90N
DEPTH (meters)
0
200
400
600
800
1000
2000
3000
4000
5000
5500
34.0
34.2
34.4
34.6
34.8
35.0
35.2
35.6
36.0
36.4
34.65
34.67
34.69
34.68
34.7
34.9
34.95
34.66
34.65

Fig 9b

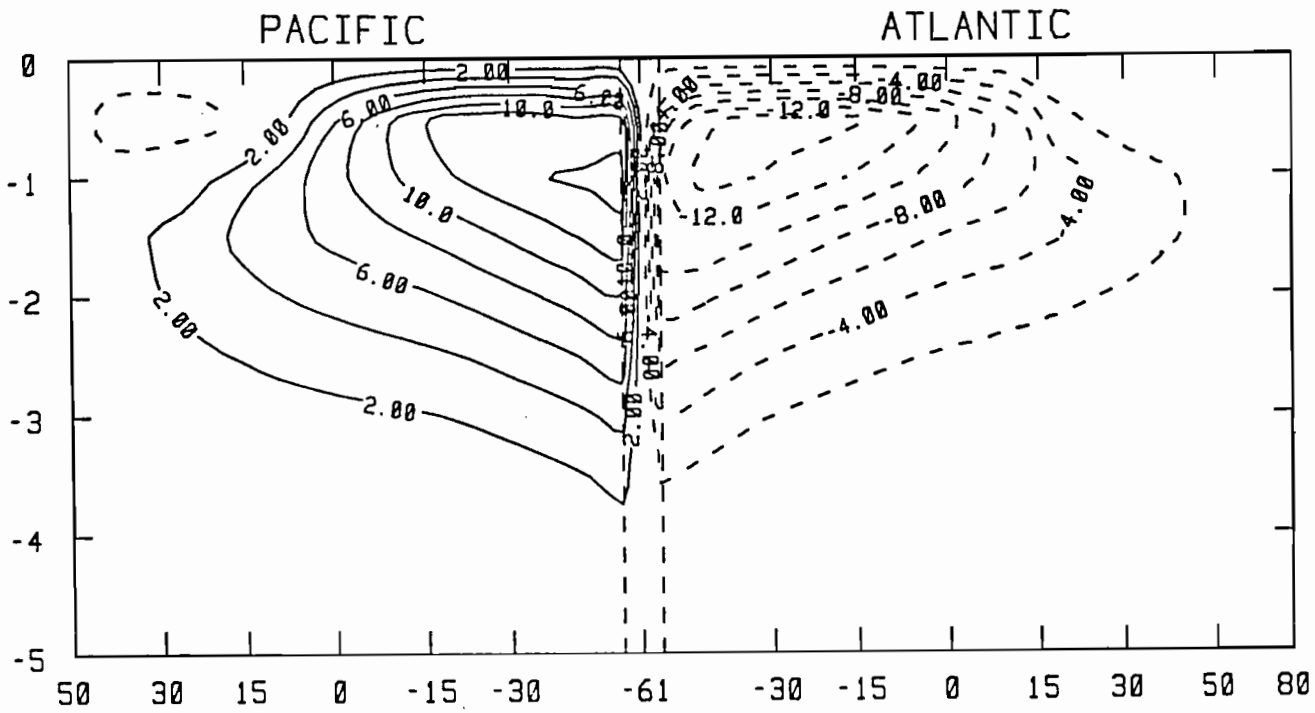

Fig 10a

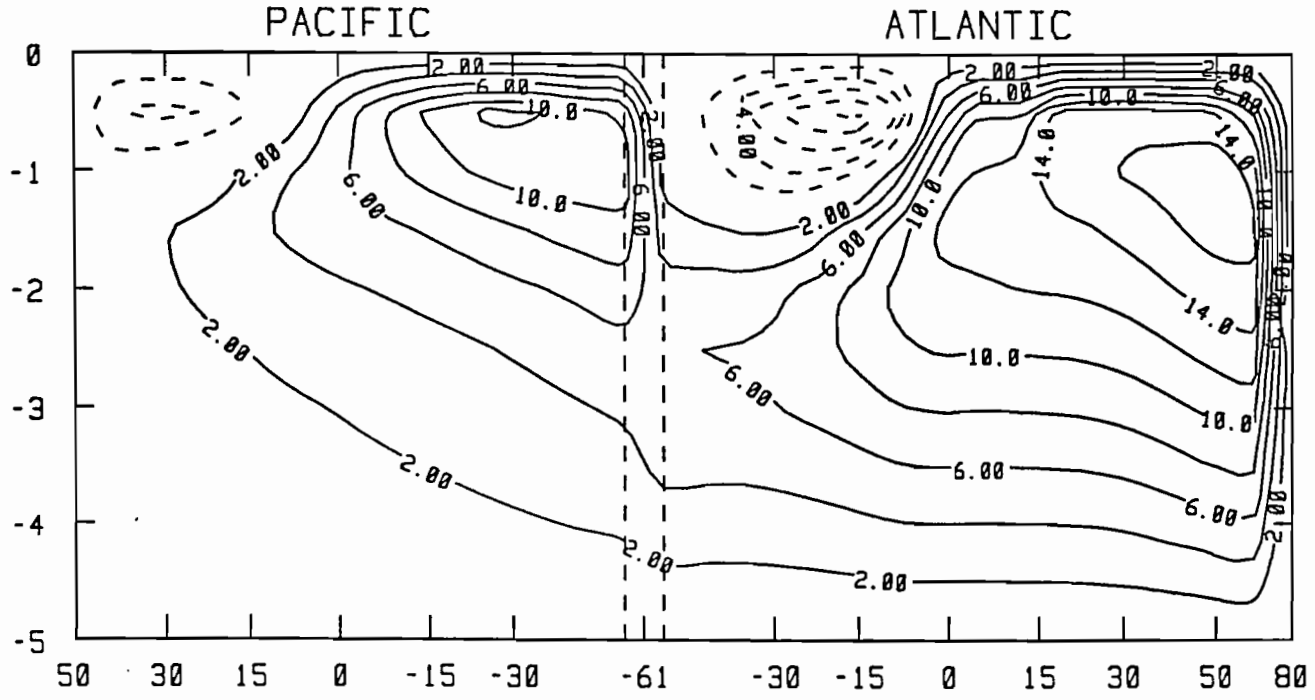

Fig 10b

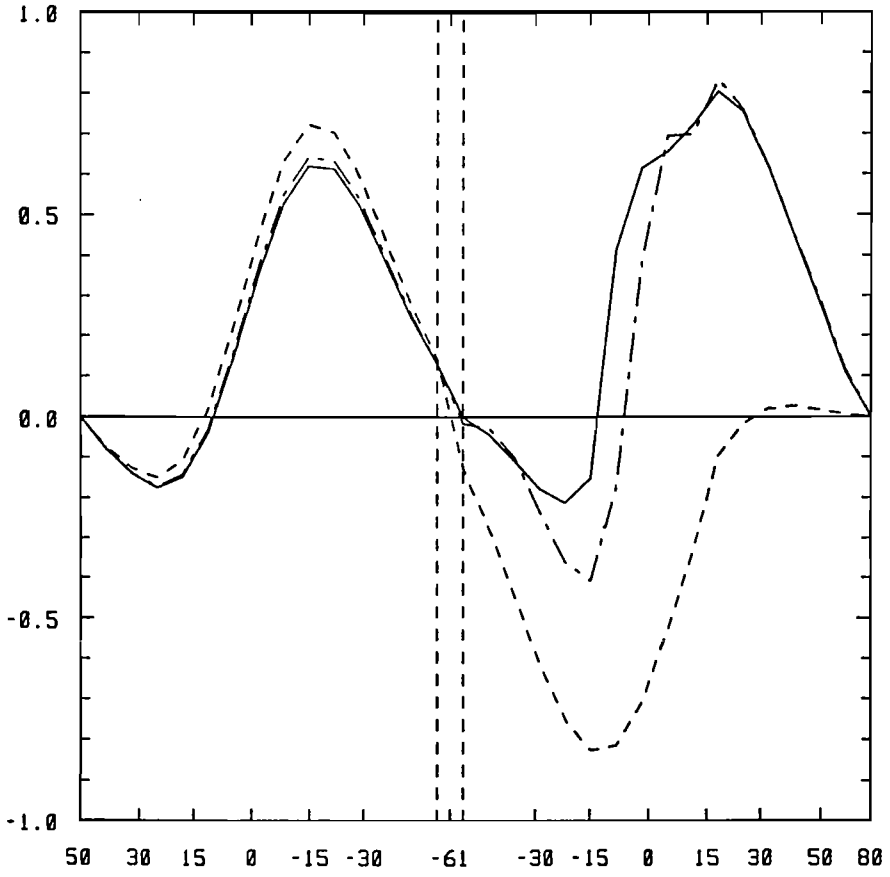

Fig 11